Assessing the variability of Aerosol Optical Depth over India in response to future scenarios: Implications for carbonaceous aerosols

Nidhi L. Anchan[1,2], Basudev Swain[3*], Amit Sharma[4], Aishwarya Singh[1,2], Chakradhar Reddy Malasani [1,2], Arundathi Chandrasekharan[1,2], Utkarsh Kumar[1,2], Narendra Ojha [5], Pengfei Liu[6], Marco Vountas[3], Sachin S. Gunthe[1,2†]

[1]Environmental Engineering Division, Dept of Civil Engineering, Indian Institute of Technology Madras, Chennai, India
[2]Center for Atmospheric and Climate Sciences, Indian Institute of Technology Madras, Chennai, India
[3]Institute of Environmental Physics, University of Bremen, Germany
[4]Department of Civil and Infrastructure Engineering, Indian Institute of Technology Jodhpur, Jodhpur, India
[5]Physical Research Laboratory, Ahmadabad, India
[6]Georgia Institute of Technology, USA

Key Points:

- The future changes in carbonaceous aerosols carry significant consequences for air quality together with climate change in India.
- Mitigation of carbonaceous aerosols is essential to maximize the co-benefits for future air quality.
- Future shifts in emissions will affect the degree of mitigation needed for anthropogenic sources over India after the year 2030.

*Germany
†Chennai, India

Corresponding author: Basudev Swain, Sachin S. Gunthe, `basudev@iup.physik.uni-bremen.de`, `s.gunthe@iitm.ac.in`

Abstract

Air pollution caused by various anthropogenic activities and biomass burning continues to be a major problem in India. To assess the effectiveness of current air pollution mitigation measures, we used a 3D global chemical transport model to analyze the projected optical depth of carbonaceous aerosol (AOD) in India under representative concentration pathways (RCP) 4.5 and 8.5 over the period 2000-2100. Our results show a decrease in future emissions, leading to a decrease in modeled AOD under both RCPs after 2030. The RCP4.5 scenario shows a 48-65% decrease in AOD by the end of the century, with the Indo-Gangetic Plain (IGP) experiencing a maximum change of ∼25% by 2030 compared to 2010. Conversely, RCP8.5 showed an increase in AOD of ∼29% by 2050 and did not indicate a significant decrease by the end of the century. Our study also highlights that it is likely to take three decades for current policies to be effective for regions heavily polluted by exposure to carbonaceous aerosols, such as the IGP and eastern India. We emphasize the importance of assessing the effectiveness of current policies and highlight the need for continued efforts to address the problem of air pollution from carbonaceous aerosols, both from anthropogenic sources and biomass burning, in India.

1 Plain Language Summary

Air pollution from human activities and biomass burning is a significant issue in India. To understand the efficacy of current efforts, a computer model is used to study the projected levels of carbonaceous aerosols (measured as optical depth) from 2000 to 2100. The results suggest that emissions are expected to decrease after 2030, leading to a drop in modeled aerosol levels. In an optimistic scenario of RCP4.5, aerosol levels could decrease by 48-65% by the end of the century, with the Indo-Gangetic Plain(IGP) showing the most improvement by 2030. However, in a scenario without any significant measures, aerosol levels may increase by 29% by 2050 and not improve significantly by the end of the century. The study indicates that it might take around 30 years for current pollution control measures to make a noticeable difference in heavily polluted regions like the IGP and eastern India. These findings underscore the importance of evaluating the effectiveness of current policies and the need to address air pollution in India caused by carbonaceous aerosols from both human activities and biomass burning. This information is crucial for policymakers and the public to understand the progress made and the challenges that persist in combating air pollution.

2 Introduction

Atmospheric aerosols are considered to be the most important air pollutants affecting human health (Butt et al., 2016; Shiraiwa et al., 2017), atmospheric visibility (Gunthe et al., 2021), precipitation patterns (Sarangi et al., 2018; Nandini et al., 2022), and regional and global climate change (Levy et al., 2013; Haywood, 2021). In recent decades, rapid economic expansion, population growth, and urbanization have led to increased concentrations of atmospheric aerosol components, including sulfate, Black Carbon (BC), Organic Carbon (OC), and dust, particularly over the Indian subcontinent (Provençal et al., 2017; David et al., 2018). In addition, Sea Salt (SS) particles are an important natural contributor to aerosol mass in coastal regions. (Murphy et al., 2019; Chin et al., 2002). These constituents play an important role in understanding the air quality over the region.

Aerosol Optical Depth (AOD) is an important optical property of aerosol particles, which can serve as a proxy for analyzing air quality. Several studies show that the daily and monthly mean AOD over heavily populated areas such as the Indo Gangetic Plain (IGP) has reached a maximum of about 0.8-0.9 (Lodhi et al., 2013; M. Kumar et al., 2018). Moreover, both light-absorbing and scattering carbonaceous aerosols (Black Carbon (BC) and Organic Carbon (OC) (Xie et al., 2017)) are increasing over India due to increased Biomass Burning (BB) and various other anthropogenic sources (Venkataraman et al., 2006; Mhawish et al., 2021). This has a positive radiative effect on climate leading to an increase in near-surface temperature (Andreae & Gelencsér, 2006; Liu et al., 2020) and suppression of monsoon rainfall (Andreae, 1993; Cowan & Cai, 2011) over India. Additionally, these fine mode (FM), OC, and BC are associated to many cardiovascular mortality and morbidity, which include lung diseases such as asthma, Chronic Obstructive Pulmonary Disease (COPD), and lung cancer (Butt et al., 2016; Yang et al., 2019). Therefore, there is growing concern among policymakers and the scientific community in India about the future increase in carbonaceous aerosols from various BB and anthropogenic emission sources and the need to reduce these future emission sources on a high priority basis(Keywood et al., 2011; Lee et al., 2017).

For this, four Representative Concentration Pathways (RCPs) were adopted in the Intergovernmental Panel on Climate Change (IPCC) Fifth Assessment Report for the future climate projections: RCP2.6, RCP4.5, RCP6.0, and RCP8.5, which represent global radiative forcing of 2.6, 4.5, 6.0, and 8.5 Watts m^{-2}(Li et al., 2016), respectively. The RCPs outline the courses of action for emissions of greenhouse gases (GHGs), atmospheric concentrations, air pollutant emissions, and land use throughout the 21st century. According to the Synthesis Report (SYR) of the IPCC Fifth Assessment Report (AR5), the four Representative Concentration Pathways (RCPs) are divided into scenarios, with RCP2.6 being the scenario with strict mitigation and lowest forcing level making it the most optimistic scenario, followed by two mid-range scenarios - RCP4.5 and RCP6.0, and finally RCP8.5, the scenario with unabated emissions, which is also likely to be a worst-case scenario. In the absence of additional measures to limit emissions, often referred to as 'baseline scenarios', our trajectory is expected to fall within the range of RCP6.0 to RCP8.5 (Intergovernmental Panel on Climate Change, 2014). Since the RCP2.6 scenario is an optimistic model, it is difficult to achieve, while RCP6.0 is between RCP4.5 and RCP8.5. Therefore, RCP4.5 and RCP8.5 are expected to cover a realistic range of the estimated future (Chowdhury et al., 2018). Furthermore, RCP4.5 is a stabilization scenario representing a plausible pathway that could potentially limit the magnitude of future climate change impacts (Chowdhury et al., 2018).

Over the last few decades, analysis using various models, satellite data, and ground-based AERONET stations have revealed an increasing trend in the temporal mean AOD over India (Ramachandran et al., 2012; Srivastava & Saran, 2017). Several studies over India and various parts of the country have pointed out the increase in AOD due to regional and long-range transport of anthropogenic aerosol components (Rawat et al., 2019; David et al., 2018; Rajeev et al., 2000). This increase in aerosol loading is attributed to urbanization and population growth, which mainly contribute to the anthropogenic contribution of aerosols in India. Seasonal variations, especially in one of the most affected regions, IGP, show a significant increase in AOD during November-December and March-April, and a decreasing trend during May-October (Alpert et al., 2012; Chawala et al., 2023). To understand the future of aerosol loading in India, few studies have attempted to estimate the change in AOD and some of its components under RCP scenarios. (Saha et al., 2017) estimated an increase of 1.42% under RCP8.5 over the Indian subcontinent by 2036-2045 compared to base-lines 1996-2005. However, not many attempts have been made to understand the future changes in carbonaceous aerosols in the Indian region.

Fossil fuel combustion and biomass burning are the two major sources of carbonaceous aerosol loading in India. The dominance of these sources over each other varies across different regions throughout the country (Dutta & Chatterjee, 2021). It is also observed that the contribution of fossil fuel emission is higher during pre-monsoon, whereas post-monsoon and winter are dominated by biomass burning in certain parts of the country (Bikkina et al., 2019). Biomass burning is closely related to emissions as well as global and regional climate change (Taylor, 2009; Reisen et al., 2013). In turn, climate change may lead to more severe fires with high frequency and high intensity (FLANNIGAN et al., 2009). The growing population may increase the total emissions from anthropogenic as well as biomass burning emissions (Perera, 2017). An approximate increase of 38% in OC and 35% in BC emissions was estimated over India during 1996-2010 (Lu et al., 2011; Rawat et al., 2019). BC aerosols from fossil fuel burning were reported to be approximately 4 times higher than biomass burning in urban regions of western India (Rajesh & Ramachandran, 2017). Literature also indicates that the largest amount of biomass burning occurs in Southeast Asia, where an estimated 330 Tg of biomass is burned in an average year. This is primarily due to a large amount of agriculture slash burn and timber harvesting carried out here (Galanter et al., 2000; Streets et al., 2003). In 1990, India's black carbon emissions were estimated at 0.45 Tg per year, of which 55% was from fossil fuel combustion and 45% from biomass combustion. Similarly, India's organic matter emissions for the same year were estimated at 2.46 Tg per year, with 43% from fossil fuel combustion and 57% from biomass combustion (Shekar Reddy & Venkataraman, 2000).In 2018, India emitted 1480 Gg yr^{-1} anthropogenic BC. Transport was the largest at 46% (673 Gg yr^{-1}), followed by residential at 26% (387 Gg yr^{-1}), and 16% (239 Gg yr^{-1}) from other sectors. Industry and thermal power composed 11% (161 Gg yr^{-1}) and 1% (19 Gg yr^{-1}), with mobile diesel and irrigation at 2% (31 Gg yr^{-1}). Simultaneously, 2018's anthropogenic organic carbon (OC) emissions hit 3116 Gg yr^{-1}. Residential biofuel burning accounted for 39% (1213 Gg yr^{-1}), transport for 32% (1010 Gg yr^{-1}), and other sources for 29% (893 Gg yr^{-1}) (P. Kumar et al., 2023).

Air pollution due to carbonaceous aerosols in India requires urgent strategies to reduce emissions, as India has set a target of net zero carbon emissions by 2070 at the UN Climate Summit Conference of Parties (COP26) in Glasgow in 2021. Over the past decade, the Indian government has adopted and implemented stringent measures to reduce air pollution (Gulia et al., 2022). The effectiveness of these measures can be assessed by analyzing changes in aerosol loading from various emission sources. To quantify the impact of these emission sources in India in the future, the current study aims to understand the seasonal variations of carbonaceous aerosol under futuristic climate scenarios. India has spatially varying landscapes, climates, and population distribution; accordingly, the study area is divided into six different regions. The objective is to understand the future evolution of carbonaceous aerosols (BC+OC) due to both anthropogenic and BB emissions under RCP4.5 (medium) and RCP8.5 (extreme) scenarios, thereby further providing deep insights into the impact and decadal trend of AOD in India up to the end of the century (the year 2100). The study excludes all climate changes that could affect the future contributions of these emission sources. Instead, the focus is solely on the impact of changes in emissions, which is the primary objective of policymakers to improve air quality in India in the future.

A description of the GEOS-Chem (GC) model, RCP scenarios, satellites, and ground-based observational data is provided in section 3. A detailed overview of the study region and its classification is presented in section 4. Section 5, compares the AOD from the model using current emission inventories with the satellite and ground-based observations. Furthermore, we compared the carbonaceous AOD from the 2010 GEOS-Chem simulation (GC_{2010}) obtained using the 2010 meteorology as well as the emissions with projected carbonaceous AOD over India under the two RCP scenarios. The seasonal changes in these AOD for different regions were also examined. Section 6 discusses implications that may be useful for policymakers, and the main findings of the study are summarized in section 7.

3 Methodology

3.1 GEOS-Chem Model description

In this study, the GEOS-Chem (GC) 3-D chemical transport model (version 12.1.1) (accessible at `https://geoschem.github.io/`, (Bey et al., 2001)) has been used. The assimilated meteorological data with 6-hour timestep has been used from Modern Era Retrospective Reanalysis2 (MERRA2) datasets (Song et al., 2018). The simulation domain is localized over Asia (11°S-55°N, 60°-150°E) with a horizontal resolution of 0.5° × 0.625° and 47 vertical layers extending down to 0.01 hPa. For aerosol chemistry, GC uses aerosols, gas-aerosol phase partitioning, and O_3-NOx-hydrocarbon chemistry. Tracer concentrations at the lateral boundaries are derived from global GEOS-Chem simulations with a horizontal resolution of 4° × 5° and an update frequency of 3 hours. The GC simulated AOD of different components such as black carbon (BC), organic carbon (OC), dust, sulfate (SO_2) and sea salt (SS), which were further aggregated to total AOD. The simulation for carbonaceous aerosols such as BC and primary OC(POC) follows standard GEOS-Chem procedures outlined by (Park et al., 2003).

Simulations are conducted utilizing emissions data representative of the present-day (year 2010) and future emissions spanning from 2010 to 2100 for each Representative Concentration Pathway (RCP) scenario. All simulations utilize the 2010 MERRA-2 assimilated meteorological dataset. The selection of the year 2010 is motivated by its relatively stable meteorological conditions (Li et al., 2016), aligning well with the objective of simulating future Aerosol Optical Depth (AOD) based on emissions spanning from 2010 to 2100 (Song et al., 2018). This choice is particularly suitable for investigations focusing on the long-term trends and climatology of aerosol emissions (Li et al., 2016). Each simulation is integrated over an 18-month period, with the initial 6 months designated as the model initialization phase for both the nested fine resolution (0.5° × 0.625°) and global coarse resolution (4° × 5°) simulations, which provide the boundary conditions.

3.1.1 Emissions

The emissions data for each decade within the Representative Concentration Pathway (RCP) scenarios, spanning from the baseline year 2000 to 2100, encompassing carbon monoxide, non-methane volatile organic compounds (VOCs), sulfur dioxide (SO_2), nitrogen oxides (NOx), ammonia (NH_3), black carbon (BC), and organic carbon (OC), were sourced from `https://tntcat.iiasa.ac.at/RcpDb`. These emissions have a spatial resolution of 0.5° x 0.5° and originate from various sources, including transportation (surface transportation, international shipping, and aviation), energy production (power plants and energy conversion), resource extraction, residential and commercial sectors, industrial activities (combustion and processing) including solvent usage, waste management (landfills, wastewater treatment, and incineration), agriculture (field waste burning), as well as grassland and forest fires.

With the exception of emissions attributed to biomass burning, shipping, and aviation, which exhibit monthly variations, the RCP emissions are generally represented as annual averages. To enhance the precision of aerosol simulations over India, monthly scaling factors for ozone (O_3) precursors, aerosol precursors, and aerosols were derived from the MIX emission dataset for the year 2010 (Li et al., 2016). Notably, for the simulation pertaining to the year 2010 in the absence of RCP scenarios, we employed MIX emission inventories in conjunction with the Modern Era Retrospective Reanalysis2 (MERRA-2) meteorological data. Throughout this investigation, these gridded monthly scaling factors are systematically applied to anthropogenic RCP emissions across all years and RCP scenarios. The anthropogenic emissions specific to India from the MIX dataset are primarily derived from the latest inventory accessible at `http://meicmodel.org.cn/?page_id=89`, widely recognized for its application in aerosol modeling studies over the Indian subcontinent.

Fig.A1 shows the changes in the sum of anthropogenic and biomass burning emissions of SO_2, NOx, NH_3, BC, and OC over India between 2000 and 2100 as a function of RCP scenarios. In 2000, there were 5.1, 3.2, 3.8, 0.5, and 1.8 Tg species per year of SO_2, NOx, NH_3, BC, and OC emissions in India, respectively. Trends for all species over the 2000-2100 period follow a similar pattern, with peak emissions for all but NH_3 occurring between 2030 - 2040 and for OC in 2050. A significant decrease is observed in emissions between 2050 and 2100 under both scenarios. SO_2 emissions in 2100 are 68% and 30% lower than in 2000 under RCP4.5 and RCP8.5 respectively.

Under RCP4.5, NOx emissions increase (decrease) by 126% (45%) in 2040 (2100) and by 115% (14%) in 2030 (2100) under RCP8.5 compared to those in the year 2000. Under RCP4.5, BC (OC) emissions decrease (increase) by 55% (143%) in 2100 compared to those in 2000. Under RCP8.5, on the other hand, both BC and OC increased by 20% and 17%, respectively, in 2100 compared to those in 2000. Under all RCP scenarios, NH_3 emissions increase steadily by 90-137% from 2000 to 2100, primarily due to increasing food demand and population (van Vuuren et al., 2011). The natural emissions are set to 2010 and follow the configurations in the typical GEOS-Chem simulation. (Sauvage et al., 2007) and (Murray et al., 2012) describe NOx emissions from lightning, while (Yienger & Levy II, 1995) describes emissions from soil. Similarly, global emission inventory was used for the NH_3 emissions from soils, plants, and oceans(Bouwman et al., 1997). Biogenic Volatile Organic Compounds (BVOCs) such as isoprene, monoterpenes plays a crucial role in the formation of secondary organic aerosols (SOA) and were determined using the Model of Emissions of Gases and Aerosol from Nature (MEGAN) (Guenther et al., 2006). The weather of 2010 affected the natural emissions of BVOCs, lightning NOx, and soil NOx over India.

3.2 Observations (AERONET, MODIS Terra and Aqua, and MERIS)

This section outlines the satellite and ground-based observations used in this study for comparison with the model data. The satellite observations include MODIS-Aqua and Terra, as well as MERIS. The AERONET dataset consists of data from five stations, as shown in Fig. 1. These datasets were regridded to the model resolution for analysis.

Satellite observations:

MODIS: Data from two Moderate Resolution Imaging Spectroradiometer (MODIS) instruments on the Aqua and Terra satellites was used in this study. The two satellites orbit in opposite directions, with Terra starting from the North and Aqua from the South. Each satellite passes over the equator at a different time: Terra in the morning and Aqua in the afternoon. AOD over land at 550 nm was obtained from the "Optical Depth Land and Ocean" product of the level 2 aerosol product (L2 collection 6). Using the Deep Blue (over land) and Dark Target (over ocean) algorithms, MODIS L2 provides complete global coverage of aerosol properties and can be accessed at https://ladsweb.modaps.eosdis.nasa.gov/archive/allData/61/MOD06_L2/. The Deep Blue algorithm estimates AOD by analyzing different wavelengths as well as surface and atmospheric feature contrast. For our analysis, the Aqua and Terra AOD data were converted to model resolution.

MERIS: The Medium Resolution Imaging Spectrometer (MERIS) is a programmable medium spectral resolution imaging spectrometer operating in the solar reflectance spectrum and carried by the European Space Agency's Envisat satellite. In the spectral range from 390 nm to 1040 nm, fifteen spectral bands with programmable widths and positions can be selected by ground command. Santer developed the aerosol retrieval technique in 2000 based on the Look-Up Tables (LUT) approach for specific aerosol size distributions with specific refractive indices. Particles are assumed to be spherical and ground reflection is assumed to be minimal (Kokhanovsky et al., 2007). The MERIS AOD retrieval used here (Mei, Rozanov, et al., 2017; Mei, Vountas, et al., 2017) has its own cloud screening procedure, aerosol type selection, and appropriate surface parameterization. Although the instrument was originally not designed for retrieval of AOD because of the absence of SWIR channels, it has been used in a number of cases and the retrieved AOD proved to be very reliable. It should be noted that the AOD product has the native resolution of the instrument, i.e., roughly 1 km^2.

AERONET Level 2 aerosol product: AERosol RObotic NETwork (AERONET) is the direct ground based AOD observations that had been cloud-screened and quality-assured (Holben et al., 1998). Level 2 data for five AERONET sites for 2010 over India was used in this study, obtained from https://aeronet.gsfc.nasa.gov/cgi-bin/draw_map_display_aod_v3?long1=-180&long2=180&lat1=-90&lat2=90&multiplier=2&what_map=4&nachal=1&formatter=0&level=3&place_code=10&year=2010. As depicted in Fig.1 and our division of regions, two of the five stations are in IGP (Kanpur and Gandhi College in Uttar Pradesh), and the rest is in NI (Nainital), SI (Pune), and WI (Jaipur). The AOD at 550nm was used for all the AERONET stations except Pune. Due to the unavailability of AOD data at 550 nm for Pune the next close wavelength of 675 nm was used in the analysis. At a resolution of 0.5° x 0.625°, the monthly averaged AERONET observations were matched to the closest GEOS-Chem grid cells.

4 Study Region

The Indian region extending between 8°4'N 68°7'E to 37°6'N 97°25'E encompasses diverse terrain, including the mountain ranges in the north, the Gangetic Plain, the deserts in the northwest, the central plateau, and the Deccan plateau with the eastern and western ghats on the sides. This diverse topography, coupled with variability in the population distribution, land use, land

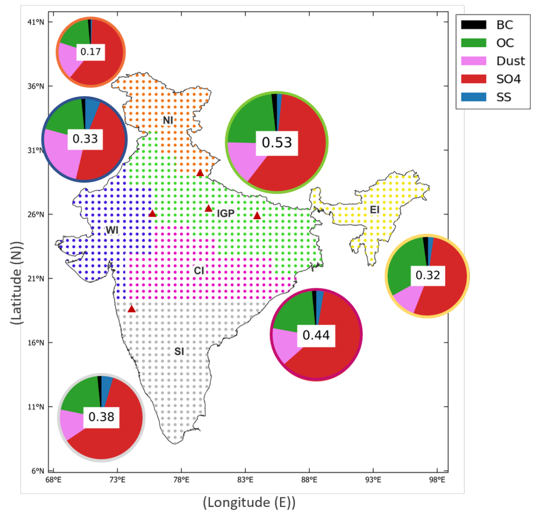

Figure 1: The study area is divided into six different domains based on climatic conditions, seasonal variability, and aerosol variations. Pie charts display the average AOD and the distribution of its components at 550nm modeled by GEOS-Chem for the year 2010, with AERONET station locations marked by red triangles.

cover patterns, and environmental conditions, contributes to the heterogeneous nature of aerosol characteristics.

The aerosol distribution over any region is intricately linked to the sources, which in turn is closely related to the demography and land use - land cover pattern. For instance, the Indo-Gangetic Plain (IGP) is one of the most populous regions of India, which could be attributed to the availability of fertile land and water resources. The region also has the highest emissions, resulting in significant amounts of various pollutants (Rawat et al., 2019; Mogno et al., 2021), with the emissions from anthropogenic origin evident in the region. Carbonaceous aerosols significantly contribute to the IGP region due to fossil fuel and coal burning, biomass burning such as wood, burning of agricultural waste, forest fires, and other anthropogenic pollution. Similarly, the western part is dominated by the dust particles from the suspension during hot and dry weather, further enhanced by long-range transport from Asian and African deserts (Mitra & Sharma, 2002; Streets et al., 2003; Dey et al., 2004; Sharma et al., 2010; Misra et al., 2014; Yadav et al., 2022).

India's climate exhibits distinct variations, primarily influenced by its geographical features. The country experiences a continental climate marked by notable seasonal changes. Southern and central regions, situated closer to the equator, undergo a tropical climate with consistently warm temperatures. In contrast, the northern and northwestern parts feature a subtropical climate characterized by relatively hotter summers and colder winters. The onset of the Southwestern monsoon, marked by prevailing southwesterly winds, impacts most of the country, while specific regions experience northeasterly winds during the reversal phase. Consequently, India's meteorological seasons are categorized into winter (December-January-February), pre-monsoon/summer (March-April-May), monsoon (June-July-August-September), and post-monsoon (October-November) (David et al., 2018; Mangla et al., 2020).

The pollution levels in a region are significantly influenced by both topography and weather conditions. The Hindu Kush and the Himalayas, situated to the northwest and northeast of the Indo-Gangetic Plain (IGP), along with its continental weather, contribute to elevated pollution levels, particularly during the winter months (Mogno et al., 2021). The pollution events in the IGP have a substantial impact on eastern India (EI) along with forest fire events in the region (Ramachandran & Cherian, 2008; Biswas et al., 2017). Conversely, southern India, enveloped by oceans on all sides, maintains a relatively cleaner environment. Emissions from other parts of India are not expected to exert a notable effect on the northern part of India (NI). For this study, India has been divided into six domains (Fig.1) based on topography, climatic conditions, seasonal variability, and variation in the aerosol distribution. In Fig.1, NI, WI, EI, CI, SI and IGP represent the northern, western, eastern, central, and southern parts of India and the Indo-Gangetic Plain, respectively. (David et al., 2018, 2019). The ground-based AERONET stations are represented by red triangles for each region.

5 Results and Discussion

5.1 Current AOD trends and its composition over India

In the following section, we discuss the distribution of AOD compositions considered for this study (such as BC, OC, dust, SS, and SO_4) across the six regions of India for the year 2010 (Fig.1). Next, we will look at the seasonal variation that would further aid in a better understanding of the dynamics of these components and the total AOD in India with different seasons.

5.1.1 Spatial distribution of AOD and Aerosol composition

The mean AOD and its components over six different regions of India for the year 2010 are shown in Fig.1. IGP region exhibited the highest average AOD followed by CI, SI, WI, EI, and NI, with a mean AOD of 0.53, 0.44, 0.38, 0.33, 0.32, and 0.17, respectively. In the six regions, the sulfate concentration is found to dominate, followed by OC, except for WI where dust dominates potentially because of the prevailing arid climate and presence of deserts (Table.1). In EI, the contribution of OC is highest amongst the six regions, and NI has the least mean AOD and is one of the cleanest regions due to its high altitude and less emission sources. Fig.2 shows the simulated seasonal mean concentration of OC, BC, dust, sulfate, SS, and Total AOD (sum of OC, BC, dust, sulfate, and SS). The highest seasonal mean AOD is observed to be 0.8 to 1.0 in some parts of IGP during post-monsoon (October-November). During this period, especially in November, the pollutants are trapped due to the shallow atmospheric boundary layers (Ojha et al., 2020). Also, the fire emission rates during the post-monsoon crop harvesting season are three times higher than during the pre-monsoon season (Mogno et al., 2021). The major contributors observed are sulfate, followed by OC. This region's industrial sector is responsible for these species' regional emissions (Rawat et al., 2019; Shukla et al., 2022). Specifically, the OC AOD is observed to be the highest in IGP. The value ranges from 0.16 - 0.2. IGP is expected to have high AOD values due to high population density and emission sources (David et al., 2018). The high concentration of carbonaceous aerosols (OC and BC) can be attributed to biomass burning emissions, whereas the secondary source could be due to the condensation of organic vapors as they oxidize and become less volatile (Seinfeld & Pandis, 2016; Mogno et al., 2021).

Further, high aerosol loading ranging between 0.5 to 0.7 is observed in IGP, EI, southwestern India, and the east coast during winter (December-January-February). It is during this period that anthropogenic activities dominate aerosol loading. Therefore, a higher AOD is observed in the peninsular region compared to the northern part in winter, which is in line with the studies conducted by (Tripathi et al., 2006). Moreover, the coal-based thermal power plant location coincides with the areas of high AOD in the central and the eastern IGP (Tyagi et al., 2021). Additionally, the highest seasonal mean AOD of 0.47 is observed in summer (March-April-May). Studies suggest that the southwesterly summer winds transport dust from the Thar Desert, and biomass burning is also a major contributor, specifically in the Western part of IGP, during this period. Additionally, the industrial sector in the eastern part is the prominent anthropogenic source and contributor (Dey et al., 2004; Shukla et al., 2022). About ∼76% of IGP forms major cultivable land. Therefore, crop residue burning after harvest is one of the major practices during this season that contributes to emissions (R. Kumar et al., 2011). During this period, the AOD is observed to be high in EI. Further, EI is highly influenced by the activities in IGP as the winds transport the pollution from IGP to EI. Several studies have reported high levels of AOD in North East India, particularly during the summer when the winds carry the pollution from the IGP region toward the eastern Himalayas (Biswas et al., 2017).

Table 1: Region wise Aerosol Composition (%) for the year 2010

Region	Aerosol Composition %				
	BC	OC	Dust	SO_4	SS
India	1.66	21.67	15.34	58.20	3.13
North India	1.44	18.66	18.93	60.28	0.70
Indo-Gangetic Plain	1.80	22.84	14.88	58.82	1.66
East India	2.15	30.90	11.04	53.56	2.34
West India	1.54	19.28	25.45	47.60	6.12
Central India	1.54	20.59	14.33	60.83	2.71
South India	1.55	20.29	12.49	61.13	4.55

Note: Percentages may not total 100% due to rounding errors.

5.1.2 Seasonal variation in AOD

In this section, the seasonal variation in GC-simulated AOD and its components, along with the satellite observations (MODIS Terra, MODIS Aqua, and MERIS) and ground-based AERONET measurements over the six regions will be discussed. The seasonal variation of AOD and its components over the six regions of India and for all the seasons of the year 2010 is shown in Fig.4. Additionally, for better understanding, we have compared the Total AOD data of GC and all

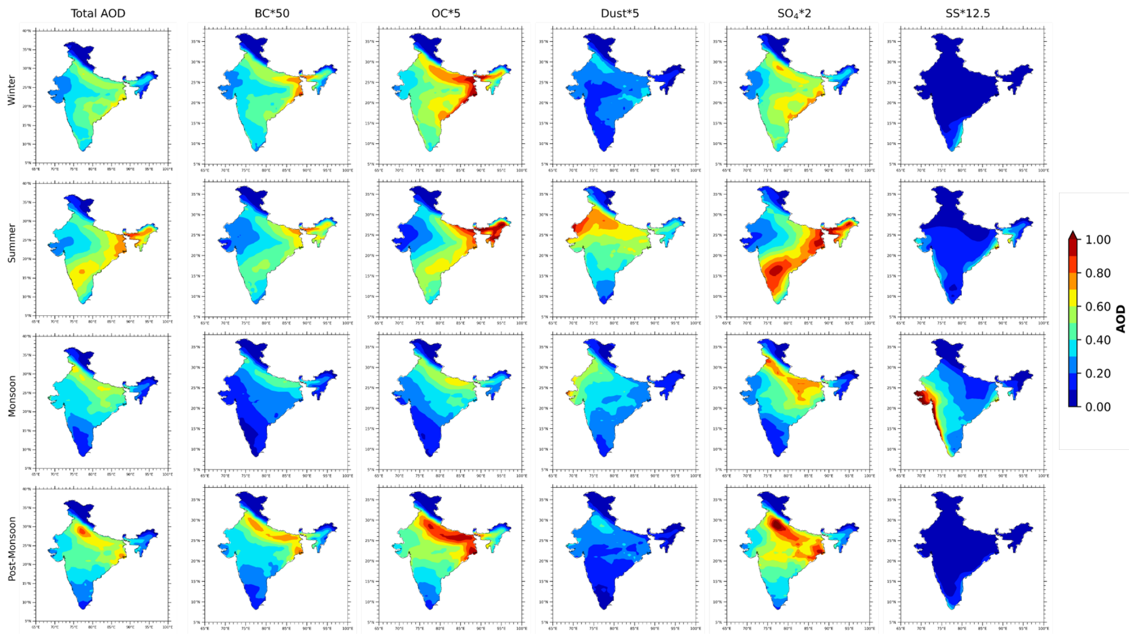

Figure 2: Spatial plot illustrating the Total AOD and its components derived from GEOS-Chem for the year 2010. The color bar represents the AOD values. The components have been scaled to a common magnitude by multiplying them with appropriate factors.

the satellites using a box and whisker plot as shown in Fig.3. The plot indicates no considerable fluctuation in the mean AOD values among the seasons.

During monsoon, the MODIS Aqua and Terra AOD are observed to be about ∼26-41 % more than the model and the MERIS AOD. It is only in this season that the modeled total AOD is lower compared to the satellites' AOD. On the other hand, the spatial resolution of MERIS is higher compared to MODIS. Additionally, the algorithm used by both instruments for estimating AOD is different. Therefore, this difference in the spatial resolution and algorithm can lead to a difference in value between MERIS and MODIS AOD. On further investigating the components, the highest contributor is observed to be sulfate, followed by dust (Fig. 4). The contribution of SS in all the regions is highest in monsoon compared to other seasons. SS contributes ∼13.3% in WI followed by ∼12.41% in SI. For the rest of the regions, it ranges from ∼1% to 6%, with NI having the lowest value. The BC ranges between ∼1%-2% for all regions and OC between ∼14%-20% for regions except EI, which is ∼29.45% this season.

Whereas, during post-monsoon, GC is found to be overestimating the AOD value by ∼6-9% and ∼21.4% (Model:0.391, MERIS: 0.322, Aqua: 0.367, Terra: 0.359) relative to the MODIS (Aqua and Terra) and MERIS data, respectively. In this season, a reduction in dust and SS percentage is observed compared to monsoon. However, a considerable increase in carbonaceous aerosols is noticed. There are a few regions like IGP and EI where a consistently high percentage of OC and BC is observed as compared to other regions, and there is an increase of ∼28.14% and ∼22.33% in BC and OC with respect to monsoon, respectively, in EI and similarly ∼50.36% and ∼38.94% in IGP. Additionally, a drastic increase of ∼93% in BC and ∼68.47% in OC is evident in WI with respect to monsoon. The percentage of dust is the least in this season compared to others in all six regions.

During winter, it is observed that the model and the MODIS Terra are in good agreement, but compared to MERIS and MODIS Aqua, the model is overestimating in the range of ∼8-30%. One of the evident findings is the highest percentage of carbonaceous aerosols is in winter compared to the rest of the seasons. Especially in EI, where BC is ∼3%, and OC is ∼41.32%, there is a considerable increase of ∼17.64% and ∼14.81% in BC and OC, respectively, with respect to post-monsoon. In this season, the highest percentage of AOD component is sulfate, followed by OC ranging around ∼47-62% and ∼23-41%, respectively. When the monthly mean AOD from the satellites and model averaged over India is compared in Fig.A2, the satellite and model data show a good agreement except for some months in the monsoon (July and August). The GEOS-Chem model produces lower AOD values than satellite data, particularly over regions with high aerosol loading Fig.A3. This could be attributed to both limitations in the model's representation of aerosol sources, transport, and cloud screening by satellite products, as during Monsoon, the Indian subcontinent is very cloudy. Further, total AOD obtained from GC and satellites show comparable variations with ground-based AERONET measurements, with satellites over-estimating during monsoon months as shown in Fig.A3.

During summer, a high monthly mean AOD can be observed in the case of both model and satellite (Model:0.469, MERIS: 0.410, Aqua: 0.416, Terra: 0.429) (Fig.3). The highest total AOD is in the month of May over India in 2010 (Fig.A2). The potential contributors for such high AOD are driven by dust in the northwest regions (Dey et al., 2004) and the dominance of sea spray aerosols (Ramachandran & Cherian, 2008; Jin et al., 2018) in the southern and western parts Fig.2. It is evident from Fig.4 that the dominant component is sulfate throughout all the regions, constituting ∼55% - 65% except in WI, where the dust is ∼42% and sulfate is slightly less, that is ∼38% in this season. Compared to other seasons, we find an overall high dust composition in all the regions. Additionally, a slight variation in SS is observed in all regions compared to the winter and post-monsoon seasons. The highest variation is observed in WI, the SS during summer is ∼4.29% which is much higher as compared to winter (∼0.32%) and post-monsoon (∼1.14%). The OC ranges from ∼15% to 20%, and BC is around 1.5%.

5.1.3 An integrated view of Aerosol composition

In this study, Fig.1 depicts the variation in AOD over the six regions of India. Here, the pie chart reflects the overall AOD and its components, and its composition is shown in Table. 1. IGP, of all the regions in India, has the greatest AOD. NI is the region with the least aerosol loading with an average AOD of ∼32 % compared to that of IGP. It's interesting to note that CI and SI also have a sizable aerosol loading. Even if there are fewer emissions in EI, there is still high aerosol loading because of transport from IGP and perhaps CI. On the other hand, IGP emissions do not seem to have a substantial impact on NI.

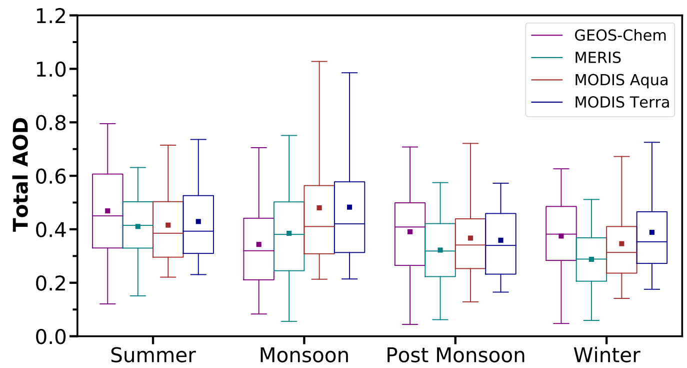

Figure 3: Box and whisker plot of total AOD (OC, BC, Dust, SS, SO4) from GEOS-Chem model at 550nm, MERIS, MODIS – Aqua, and Terra for the four seasons over India. The central line represents the median, and the square denotes the mean. The box encompasses the interquartile range (25th to 75th percentiles), while the whiskers extend to the outer percentiles (5th to 95th)

The composition of the aerosols is a crucial aspect of their distribution over India (1). Dust and sea salt have a significant influence on WI. In fact, dust contributes just as much as inorganic aerosols (anthropogenic). However, sea salt makes up a small portion of the aerosols in all the other locations, which are dominated by inorganic aerosols. The largest loading of carbonaceous aerosols is found in EI, which is a considerably less developed region. It is significant to highlight that the overall AOD over a large portion of India is affected by the sum of BC and OC, which is ∼20-33%. The sources of BC and OC are mainly anthropogenic, indicating the prevalence of human-made emissions in India.

Evaluating the modeled aerosol composition with the observations would be very helpful to comprehensively examine the model's ability to represent aerosol speciation over India. The components of aerosols have been measured in various ways from different campaigns and sites (Singh et al., 2016; Yadav et al., 2022; B. Kumar et al., 2016). Measurements have revealed that BC contributes significantly to megacities and big cities. Numerous observations also reveal that sulfate and nitrate aerosols are present in large quantities along with the prevalence of dust (Dey et al., 2004; Misra et al., 2014; Mitra & Sharma, 2002; David et al., 2018; Thiemens & Shaheen, 2014). It is pertinent to note that the emissions are continually changing, thereby making it difficult to compare the modeled data with the observations.

5.1.4 Comparison of GC, Satellite and AERONET AODs

In Fig.A4, the simulated monthly averaged AOD from GC is compared with the satellite data for 2010 over the entire India. The simulated AOD is observed to be lower than that of the measured. The calculated AOD is approximately 90% of the measured values, as determined through linear regressions that constrained the lines to pass through the origin. Taking into account the inherent measurement errors and the variability in aerosol concentrations, there is a notable

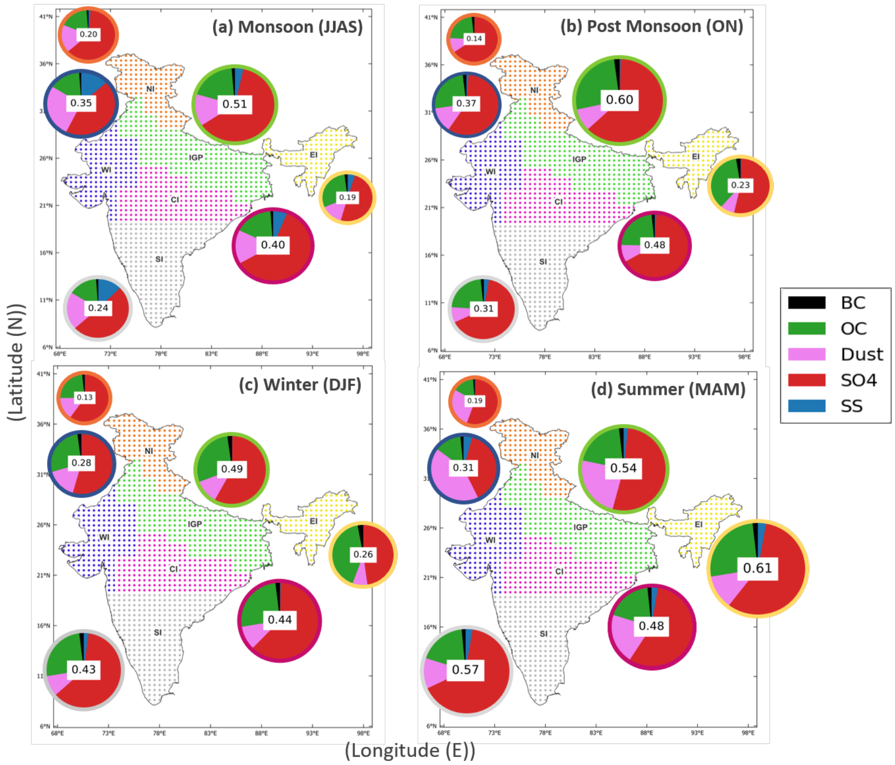

Figure 4: Seasonal distribution of AOD and its components across six regions in India. The pie chart showcases the distribution of AOD and its composition at 550nm, simulated by the GEOS-Chem model for the year 2010. The numbers within each pie represent the average AOD calculated for each region and season: (a) Monsoon, (b) Post Monsoon, (c) Winter, and (d) Summer.

agreement between the simulated and observed AOD values. A bias, or a finite estimated value when the measured value is zero, is suggested by a linear regression where the intercept is not set as zero. The Pearson correlation coefficient (R) values obtained are 0.56, 0.59, and 0.51 for MODIS Aqua, MODIS Terra, and MERIS, respectively, for AOD ≤ 1.5 as shown in Table.A1. Similarly, the slope values obtained for MODIS Aqua, MODIS Terra, and MERIS are 0.5, 0.54, and 0.53, respectively.

In Fig.A5, the GC simulated AOD is compared with satellite observations and ground-based AERONET measurements with the help of the Pearson correlation coefficient (R), the slope, intercept, and the number of data points. Due to the possibility that the satellite trajectory may not consistently align directly over the AERONET station, the satellite measurements and the GEOS-Chem model data within a 25 km radius around the AERONET station were compared, as described in (David et al., 2018) to enhance the number of available observations. A good correlation with a coefficient ranging between ~0.65 to 0.74 is observed. Several factors, such as spatial resolution, retrieval algorithm, and aerosol vertical distribution, can be attributed to the same. This comparative assessment provides a preliminary insight into the extent of coherence between observational and model data.

5.2 Current and Projected carbonaceous aerosols over India under RCP Scenarios

In this section, first, the GC_{2010} is compared with the RCP projected total AOD as well as just carbonaceous aerosols (OC and BC) for 2010 in India. This will give insights into the variations in AOD under different RCP scenarios for the same year of 2010. Next, we look into the evolution of carbonaceous aerosols and the seasonal variation that is being projected by the model. This aims to understand the contribution of OC and BC AOD under two different future RCP scenarios of 4.5 and 8.5.

5.2.1 Comparisons of current and projected AOD for 2010

The comparison of the GC simulated total AOD (OC, BC, Dust, SO_4, SS) for current (for the year 2010) with the RCP4.5 and RCP8.5 is shown in Figure 5. It is observed that for NI, EI, and WI the values are in good agreement. There is not much difference between the mean values of both RCPs. Over NI, EI and WI, the GC_{2010} mean is ~27-29% (GC_{2010}: 0.170, RCP4.5: 0.134, RCP8.5: 0.131), ~27-28% (GC_{2010}: 0.317, RCP4.5: 0.248, RCP8.5: 0.247) and ~19-23% (GC_{2010}: 0.327, RCP4.5: 0.273, RCP8.5: 0.265) respectively higher as compared to the projected values. A large difference is observed in the GC_{2010} and the projected AOD in the case of IGP, CI, and SI. Over IGP, CI, and SI, the GC_{2010} mean is ~30-35% (GC_{2010}: 0.528, RCP4.5: 0.406, RCP8.5: 0.391), ~35-42% (GC_{2010}: 0.445, RCP4.5: 0.329, RCP8.5: 0.314) and ~38-43% (GC_{2010}: 0.383, RCP4.5: 0.278, RCP8.5: 0.268) respectively higher with respect to the RCPs. Under the RCP4.5 and RCP8.5 scenarios, emissions and atmospheric chemistry changes can lead to differences in the concentration and distribution of aerosols in the atmosphere, which can affect AOD. In total AOD, a higher value of RCP4.5 is observed compared to RCP8.5.

5.2.2 Comparison of simulated current and projected carbonaceous aerosols for 2010

Comparison of the GC_{2010} carbonaceous aerosols (sum of OC and BC) with the RCP4.5 and RCP8.5, over the six regions for the year 2010 is shown in Fig. 6. The mean value for NI is seen to be in good agreement, which is ~24-26% (GC_{2010}: 0.034, RCP4.5: 0.027, RCP8.5: 0.027) higher with respect to RCPs. The mean values of GC_{2010} for EI and WI are ~27-31% (GC_{2010}: 0.105, RCP4.5: 0.08, RCP8.5: 0.083) and ~36-38% (GC_{2010}: 0.068, RCP4.5: 0.049, RCP8.5: 0.050) higher with respect to RCPs, respectively. Overall, the mean values of RCP8.5 are higher than RCP4.5, and this is consistent over all the six regions. However, it can be observed that the simulation without RCPs is comparatively higher than the RCPs for IGP (GC_{2010}: 0.130, RCP4.5: 0.092, RCP8.5: 0.098), CI (GC_{2010}: 0.098, RCP4.5: 0.060, RCP8.5: 0.068) and SI (GC_{2010}: 0.084, RCP4.5: 0.053, RCP8.5: 0.060). The GC_{2010} mean is ~33-41% for IGP, 44-63% for CI, and 40-58% for SI higher with respect to the means of both RCPs.

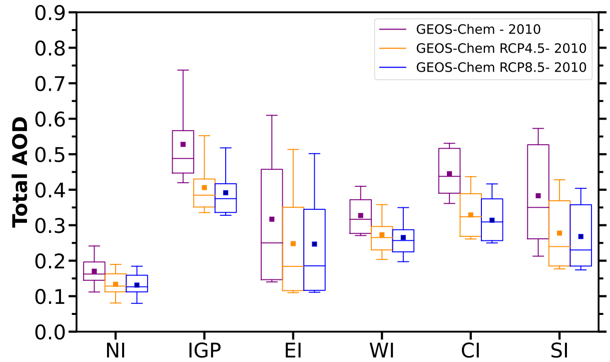

Figure 5: Box and whisker plot of total AOD (OC, BC, Dust, SO4, SS) from GEOS-Chem model at 550 nm, RCP4.5 and RCP8.5 over the six regions for the year 2010. The central line represents the median, and the square denotes the mean. The box encompasses the interquartile range (25th to 75th percentiles), while the whiskers extend to the outer percentiles (5th to 95th)

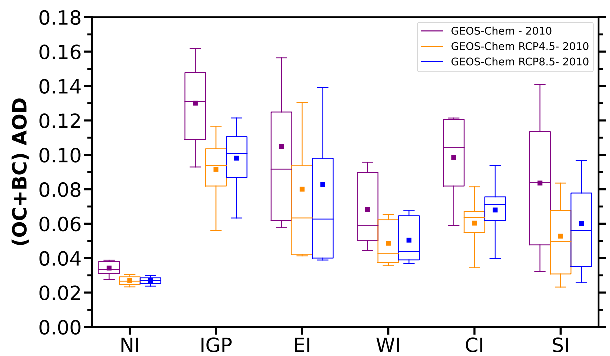

Figure 6: Box and whisker plot of Carbonaceous AOD(OC+BC) from GEOS-Chem model at 550 nm, RCP4.5 and RCP8.5 over the six regions for the year 2010. The central line represents the median, and the square denotes the mean. The box encompasses the interquartile range (25th to 75th percentiles), while the whiskers extend to the outer percentiles (5th to 95th)

5.2.3 Projected evolution of carbonaceous aerosols

In Fig.7, it could be observed that under the RCP4.5 scenario, the carbonaceous AOD is increasing at the rate of 6.91% AOD per decade up to the year 2030 and then there is a decline of -8.76% AOD per decade. On the other hand, RC8.5 showed an increase of 8.72% AOD per decade up to 2050 and further reduces by -3.52% AOD per decade from 2050 until the end of the century. Fig.8 shows the spatial distribution of the carbonaceous AOD over India and the decadal variation under the two RCP scenarios. The maximum AOD is observed over IGP in both scenarios. Under

RCP8.5, 2020-2080 is the period with high AOD, mostly contributed by IGP and EI. A gradual increase in AOD over CI and some parts of SI and WI from 2030 is noticed, but the reduction in this region is also very much evident from 2090 until the end of the century. Similar to RCP8.5, high AOD is observed over IGP and EI until 2050 in RCP4.5, however a much higher reduction by the end of the century is evident in this scenario. Unlike RCP8.5, the WI and SI remain not much affected in RCP4.5, but a high AOD on the east coast of CI and SI is apparent, which is later significantly reduced.

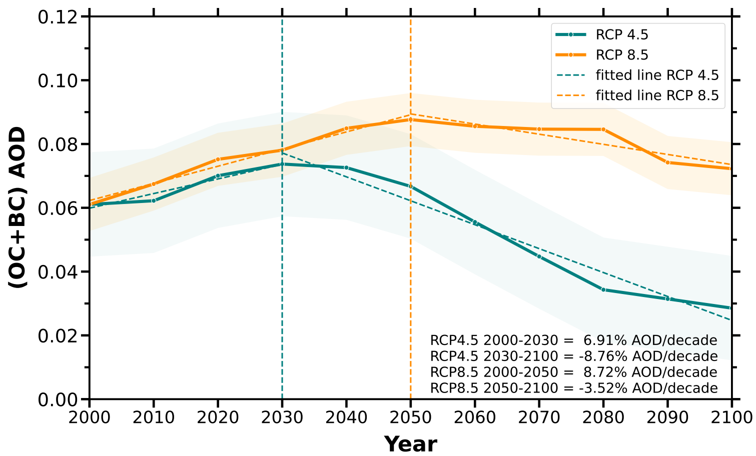

Figure 7: Time series of Carbonaceous AOD (OC and BC) at 550 nm from GEOS-Chem from 2000 to 2100 (Yearly Mean)

5.2.4 Projected changes in the seasonal mean of carbonaceous aerosols over distinct regions

Carbonaceous aerosols from both anthropogenic and biomass burning emissions in the current situation are arguably the biggest threat to air quality in the Indian subcontinent. In India, burning biomass for domestic purposes, burning solid waste, burning coal for energy, industrial emissions, burning crop residue, engaging in construction and demolition work, engaging in vehicular activity, and operating brick kilns are the main contributors to atmospheric particulate matter (Reisen et al., 2013; Lee et al., 2017; Group et al., 2018). For many years, the Indian government has placed a strong emphasis on lowering air pollution in order to achieve a cleaner environment. However, in the past ten years, some strict policies relating to air pollution have been applied and implemented across India to lower air pollution (Gulia et al., 2022). The effectiveness of such policies can be effectively judged by analyzing carbonaceous aerosols generated from emissions. This section focuses on the evolution of AOD contributed by carbonaceous aerosols over six regions. In Fig.9, the analysis of the sum of OC and BC AOD from 2020 to 2100 relative to 2010 over 6 regions under the two RCP scenarios of 4.5 and 8.5 for all the seasons is carried out.

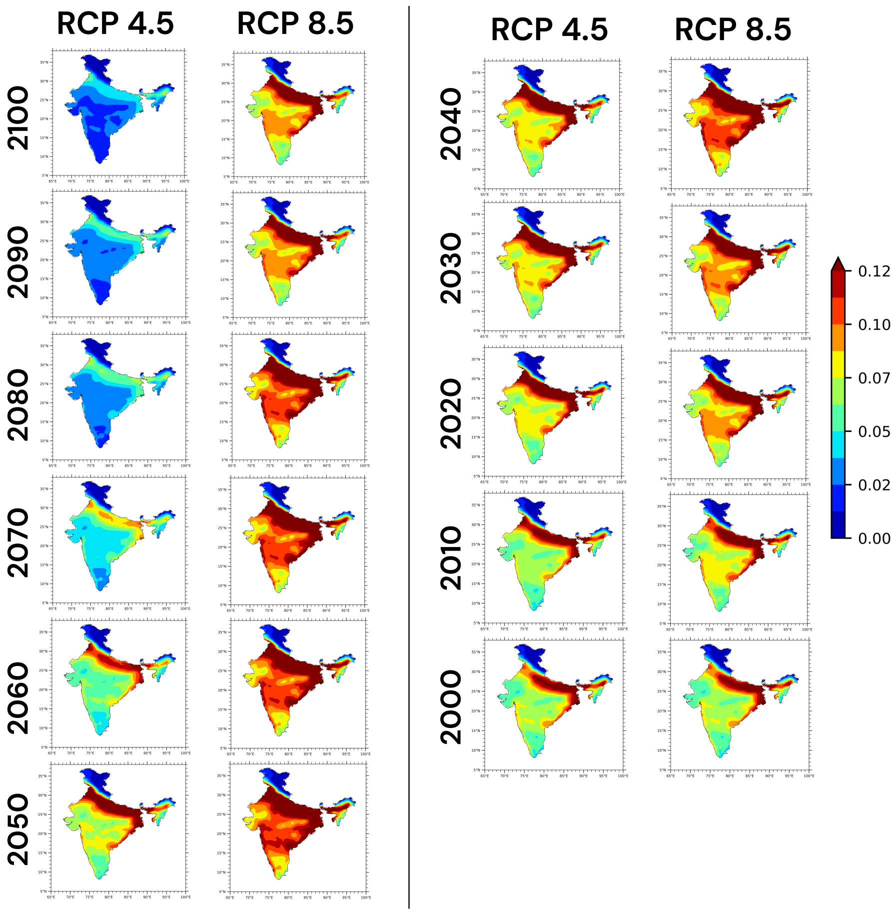

Figure 8: Spatial Decadal plot of Carbonaceous AOD (BC+OC) from GEOS-Chem for the RCP4.5 and RCP8.5. The color bar represents the (BC+OC) AOD values

NI: The analysis reveals that out of all the six regions, NI is one of the cleanest as seen in Fig.9. It could be noted that there is both positive and negative change under RCP4.5. However, in the case of RCP8.5, we could only observe a positive change. In the case of RCP4.5, the year 2030 is the year with maximum AOD for all seasons, except for the monsoon season for which the year is 2040. The maximum percentage change under RCP4.5 for monsoon, post-monsoon, winter, and summer is ∼24%, 26%, 24%, and 20%, respectively. Similarly, the maximum negative percentage for monsoon, post-monsoon, winter, and summer with respect to 2010 is ∼ (-44%, -53%, -56%, and

-36%), respectively. The year with the least AOD is found to be the end of the century, that is, 2100. Under RCP8.5, 2050 is the year of maximum AOD for all seasons. The maximum change is found to be ∼ 31%, 39%, 39%, and 28% for monsoon, post-monsoon, winter, and summer, respectively.

IGP: IGP has the highest AOD out of all the six regions (Fig.1). Under the RCP4.5 scenario, 2030 is observed to be the year with the highest AOD across all four seasons (Fig.9). However, in the case of RCP8.5, the highest AOD is observed in the year 2050 for all seasons except monsoon, where the highest value is in 2030. Among the RCP the maximum increase is observed in RCP8.5 of about ∼38% during winter. The maximum decrease is ∼(-65%) during winter under RCP4.5. Fig.4 indicates that it is during post-monsoon and winter IGP observes a high fraction of OC and BC. As for percentage changes under the RCP4.5 scenario, the maximum (minimum) values are +25% (-63%) and +27%(-65%) in post-monsoon and winter of 2030 (2100) respectively. The maximum percentage change for RCP4.5 (RCP8.5) during monsoon, post-monsoon, winter, and summer is ∼21%(21%), 25%(35%), 27%(38%) and 19%(29%) respectively. However, except for monsoon in the case of RCP8.5, a negative change is not observed as the lowest AOD value of 2100 is still ∼6-10% higher with respect to 2010.

EI: It is well established from the previous sections that due to meteorological effects, EI is highly influenced by IGP. Unlike other regions, it is evident in Fig.9 that the year with maximum AOD is 2020 for monsoon and summer, which is earlier as compared to the other seasons for RCP4.5. Similarly, for RCP8.5, the year with maximum AOD is 2040 for summer and 2050 for the rest of the seasons. The maximum percentage change, in the case of both the RCPs is the least in all the regions. The maximum(minimum) percentage change for RCP4.5 is ∼11%(-55%), 8%(-59%), 12%(-56%), and 10%(-42%) for monsoon, post-monsoon, winter and summer respectively. Similarly, for RCP8.5 the values are ∼22%, 14%(-7%), 20%(-2%) and 8%(-17%) for monsoon, post-monsoon, winter and summer respectively.

WI: The years with maximum carbonaceous AOD for RCP4.5 and RCP8.5 is 2030 and 2050, respectively, consistent for all seasons. ∼25% is the maximum percentage change that is observed in this region for the winter season under RCP4.5. Similarly, ∼39% is the maximum percentage change for the winter and summer seasons, under RCP 8.5. The AOD is expected to go as high as 0.085, which is ∼23% higher as compared to the lowest value of 0.069 observed in 2100 under the RCP8.5 scenario. The maximum negative percentage change under RCP4.5 in this region is ∼(-58%) observed in winter, followed by -55% in post-monsoon.

CI: Similar to WI the maximum AOD for RCP4.5 and RCP8.5 is 2030 and 2050, respectively and it is consistent for all seasons. The maximum positive (negative) change under RCP4.5 with respect to 2010 is ∼ 21%(-63%) in winter(post-monsoon). Similarly, for RCP8.5 the maximum AOD change is seen in 2050 (year with maximum AOD) with respect to 2010. The change is 36% in winter, followed by 33% in post-monsoon. Under RCP8.5, the least AOD due to only carbonaceous aerosols is seen in 2100 and is 0.052, 0.081, 0.091, and 0.084 for monsoon, post-monsoon, winter, and summer which is slightly higher or equal; than the reference year of 2010 which is 0.048, 0.075, 0.081 and 0.078 respectively.

SI: WI and SI are observed to be quite similar, as the maximum AOD for RCP4.5 and RCP8.5 is in 2030 and 2050, respectively and it is consistent for all seasons. There is not much difference observed between the percentage values of both regions. The maximum positive (negative) percentage change for monsoon, post-monsoon, winter, and summer for RCP4.5 is ∼14% (-46%), 18%(-62%), 20%(-63%) and 12%(-46%) respectively. Similarly, for RCP8.5, The maximum percentage change for monsoon, post-monsoon, winter, and summer is 26%, 31%, 34%, and 25% with respect to 2010.

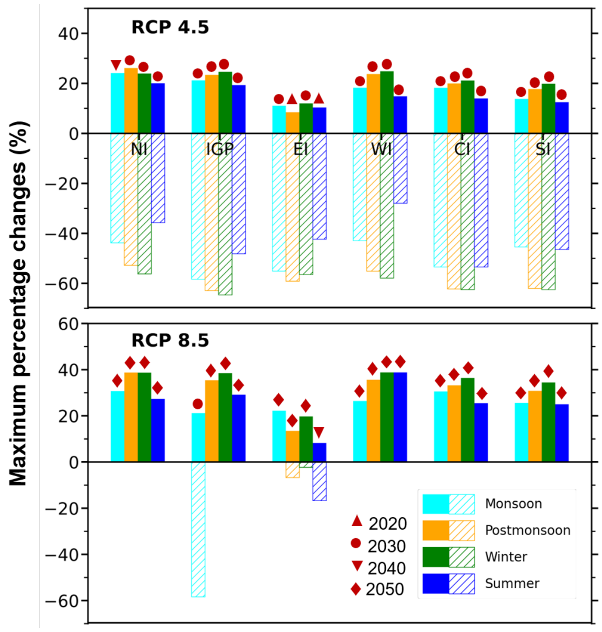

Figure 9: Shown are the maximum percentage changes (units: %) in the projected seasonal mean carbon aerosol optical depth (AOD) from 2020 to 2100 relative to the base year 2010. Plots include six regions under both RCP4.5 and RCP8.5 scenarios. Colored columns indicate maximum increases and shaded columns indicate maximum decreases. Years with notable increases are highlighted in red, while instances of maximum decreases are uniformly related to the year 2100.

6 Implication for mitigation of carbonaceous aerosol

India pledged to strive towards achieving net zero carbon emissions by 2070 at the United Nations COP26 in 2016 to control the anthropogenic emission-induced warming of the atmosphere, aligning with the goal to limit the global temperature increase to 2°C by 2100 (compared to the pre-industrial time), signed at the Paris Agreement. To achieve this aspirational target, intense emission control measures must be adopted for GHGs and particulate pollutants, especially carbonaceous aerosols. RCP scenarios representing the net radiative forcing by 2100 under different future emission patterns (as outlined in the SRES scenarios introduced in IPCC AR5) of GHGs and other climate-forcing agents based on changes in driving factors, such as economic and technological advancements, serve as useful tool for understanding the effects of emissions on future concentrations. The IPCC identifies RCP2.6 and RCP4.5 as the two most likely scenarios to achieve these objectives; however, with current mitigation policies, RCP2.6 is extremely difficult to follow. In this study, we have estimated the future levels of carbonaceous AOD (sum of OC and BC) under RCP scenarios RCP4.5 and RCP8.5 (most probable emission pathways) using the GEOS-chem model, which is shown to capture the atmospheric chemistry and transport of aerosol particles reasonably well. An increase in AOD over EI due to the outflow of aerosols from IGP shows that atmospheric transport, in addition to emission, is critical for deciding future concentrations. Our study emphasizes that aerosol loading can be significantly reduced to meet the objectives of the Paris Agreement if emissions are cut down in accordance with RCP4.5. Further, we show that if no stringent emission control measures are adopted (RCP8.5), the emission reduction will not be sufficient to limit the temperature rise to 2°C by the end of the century. By analysing the trends in potential future levels of carbonaceous aerosols across different regions of India presented in this study, policymakers can make more informed decisions about framing policies to reduce AOD levels and mitigate their radiative effects on climate change.

7 Conclusions

The study used the high-resolution nested-grid version of the GEOS-Chem (GC) model ($0.5^\circ \times 0.625^\circ$) to investigate the future trajectory of Aerosol Optical Depth (AOD) attributed to carbonaceous aerosols over six delineated regions of India from 2000 to 2100. This investigation aimed to identify the projected shifts resulting from the anticipated changes in emissions under the two RCP scenarios. The simulated GC_{2010} carbonaceous aerosol load adequately reflects the spatiotemporal distributions of observed levels in India. In addition, the GC performed well in the current simulation compared to the satellite data (with a slope and correlation coefficient of ≥ 0.93 and $\sim$0.93 to 0.95, respectively) as shown in Fig.A4 and Table.A1. When comparing the simulated AOD data with the satellite data over the 5 AERONET stations, the correlation coefficient ranged from $\sim$0.65 to 0.74. Modeled AOD showed good agreement with the retrievals of the satellite instruments, confirming the usefulness and validity of the GC model results. Moreover, the GC_{2010} simulated carbonaceous aerosols (OC + BC) also agree well with the future RCP scenarios simulation, with slight overestimation in all six different regions of India.

The GC results show an improvement in the future AOD due to carbonaceous aerosols. It could be observed that under the RCP4.5 scenario, the AOD increases at a rate of 6.91% AOD per decade until 2030, and then there is a decrease of -8.76% AOD per decade. For the RC8.5 scenario, on the other hand, an increase of 8.72% AOD per decade through 2050 and a further decrease of -3.52% AOD per decade from 2050 to the end of the century is observed.

The spatial distribution of AOD (OC+BC) across India and the decadal variation under the two RCP scenarios show that the maximum AOD is observed over IGP in both scenarios. Under RCP8.5, the period 2020-2080 is the period with high AOD mainly driven by IGP and EI. From 2030, a gradual increase in AOD is also observed over CI and some parts of SI and WI, but the decrease in this region is also very significant from 2090 to the end of the century. Similar to RCP8.5, high AOD is observed over IGP and EI through 2050, but a much steeper decline is observed in this scenario by the end of the century. Unlike RCP8.5, WI and SI are not very affected in RCP4.5, but we definitely observe a high AOD on the east coast of CI and SI, which later declines significantly.

Further study reveals that the maximum percentage increase in AOD is $\sim$25% in IGP during post-monsoon in 2030 with respect to 2010, under RCP4.5. However, the percentage increase in EI during post-monsoon is the least, which is $\sim$8% in 2020 with respect to 2010. On the other hand, it is under this scenario, a percent decrease of $\sim$30-65% could be noted by the end of the century with respect to 2010 across all four seasons, with IGP having the highest decrease. This suggests a significant reduction in AOD due to both anthropogenic and biomass-burning sources by the end of the century with respect to 2010. Under the RCP8.5, a maximum change of $\sim$40% mostly during post-monsoon and winter was observed across all the regions except for the EI where change is comparatively less. However, the decrease in AOD by 2100 with respect to 2010 is only evident in IGP during monsoon and EI during post-monsoon, winter, and summer. This indicates that the AOD for the rest of the regions and seasons under the RCP8.5 scenario will be much higher by the end of the century compared to 2010.

While the insights gained from projected future changes in the AOD of carbonaceous aerosols under RCP scenarios are valuable for informing mitigation strategies, it is crucial to recognize the inherent uncertainties associated with such projections. In particular, this study did not consider the potential impacts of future interannual to decadal climate change on the combined effects of organic carbon (OC) and black carbon (BC). Acknowledging these uncertainties underscores the need for ongoing research and refined modeling approaches to enhance the accuracy and comprehensiveness of our projections. In addition, the fully coupled chemistry-climate model estimates that combine the effects of future emissions and climate change on (OC+BC) AOD are needed. In addition, predictions of AOD levels are also influenced by regional meteorology (Reisen et al., 2013), which raises further issues that needs to be addressed.

Appendix A Additional Figures

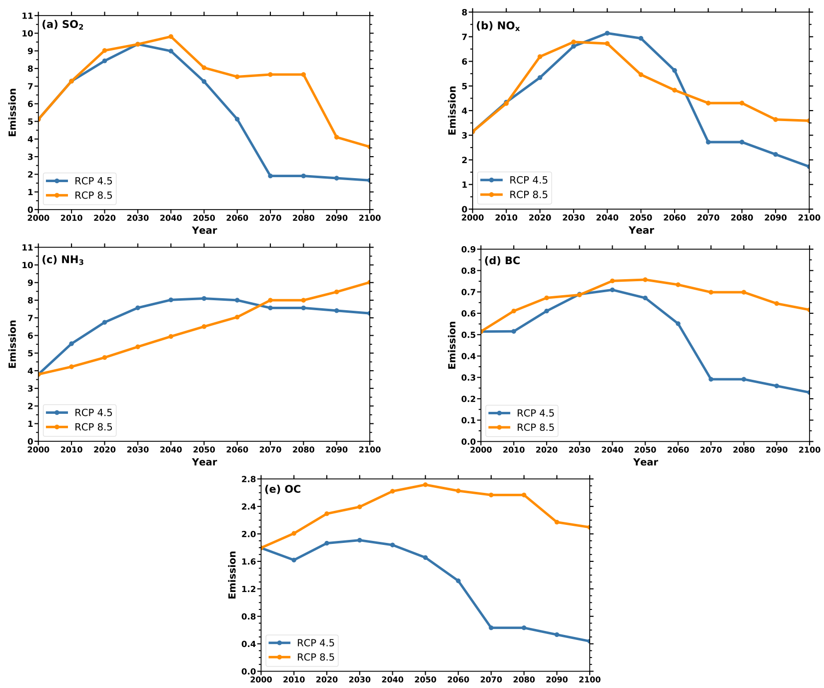

Figure A1: Sum of anthropogenic and biomass burning emission (units: Tg/year) of (a) SO2 (b) NOx (c) NH3 (d) BC and (e) OC in India for the period 2000 – 2100 under the RCP4.5 and RCP8.5

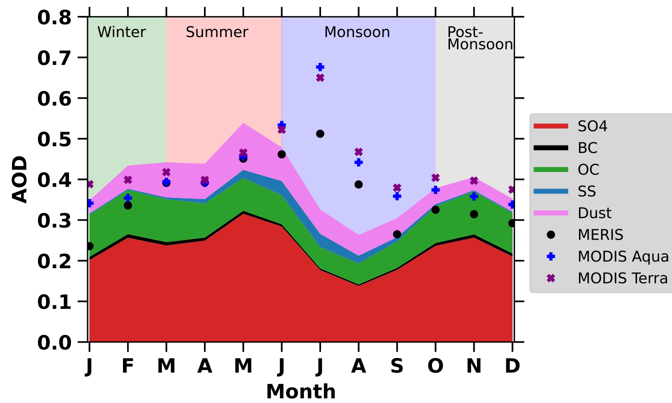

Figure A2: Monthly variation of all AOD components at 550 nm from GEOS-Chem of 2010 over India along with the monthly mean of the data from MERIS, MODIS Aqua and MODIS Terra

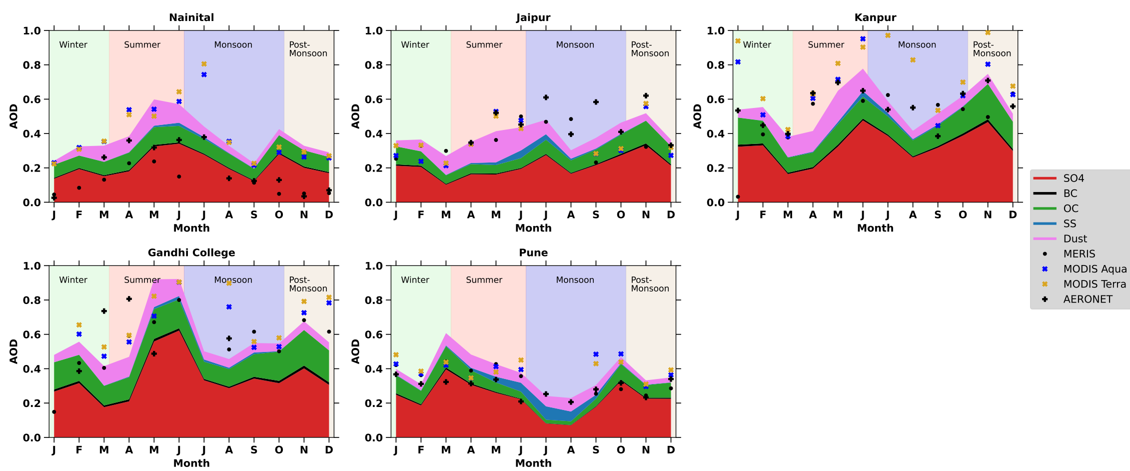

Figure A3: Monthly variation of all AOD components at 550 nm from GEOS-Chem of 2010 for the 5 AERONET station along with the monthly mean of the data from MERIS, MODIS Aqua, MODIS Terra, and AERONET Station

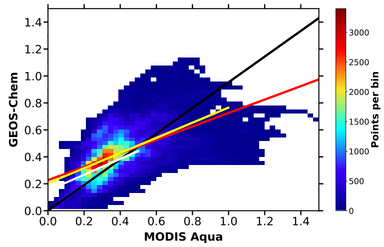

(a)

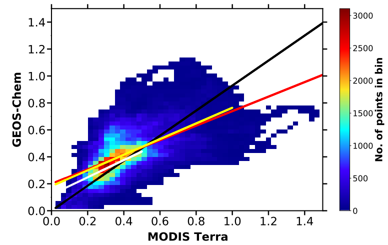

(b)

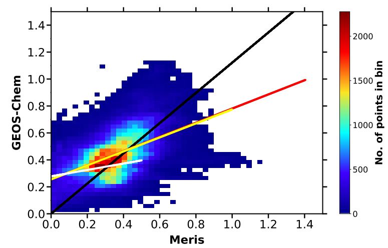

(c)

Figure A4: Density plot of simulated AOD at 550 nm with Aqua, Terra, and MERIS for 2010. The color bar represents the number of data in each 0.03 bin. The linear regression line is shown for AOD data limited to 0.5 (white), 1.0 (yellow), 1.5(red), and zero intercepts (black).

Table A1: The slope, correlation coefficient (R), and intercept (c) of simulated AOD with MODIS Aqua, MODIS Terra, and MERIS for the AOD limiting values of 0.5, 1.0, and 1.5 at 550 nm along with the slope of the line with intercept set to zero

AOD	MODIS Aqua			MODIS Terra			MERIS		
	Slope	R	c	Slope	R	c	Slope	R	c
1.5	0.95	0.93	0	0.93	0.94	0	1.12	0.93	0
1.5	0.5	0.56	0.23	0.54	0.59	0.18	0.53	0.51	0.26
1.0	0.56	0.57	0.2	0.58	0.59	0.18	0.52	0.51	0.26
0.5	0.59	0.52	0.15	0.64	0.56	0.12	0.24	0.29	0.28

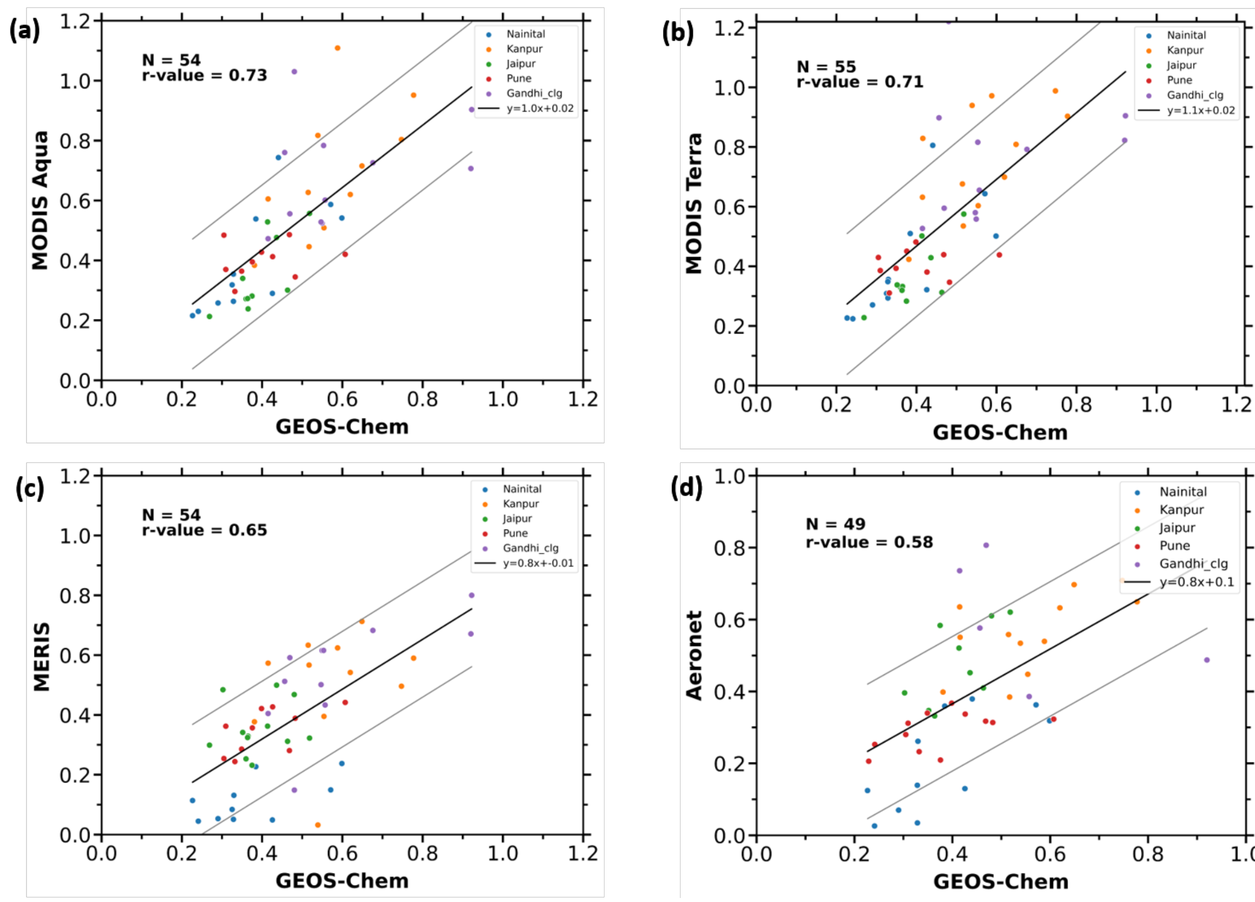

Figure A5: Correlation of GEOS-Chem with the satellite and AERONET data. The data points of both GEOS-Chem and Satellite are extracted over a 25 km radius from each AERONET station.

Appendix B Open Research

The AOD data from Aqua/MODIS and Terra/MODIS Aerosol Product 5min L2 Swath 10km, C6, NASA Level-2 and Atmosphere Archive and Distribution System (LAADS) Distributed Active Archive Center (DAAC) Goddard Space Flight Center, Greenbelt, MD are available at https://ladsweb.modaps.eosdis.nasa.gov/archive/allData/61/MOD06_L2/[MOD06_L2]. The MERIS data were obtained from Copernicus Climate Change Service, Climate Data Store, (2019): Aerosol properties gridded data from 1995 to present derived from satellite observation. Copernicus Climate Change Service (C3S) Climate Data Store (CDS) https://doi.org/10.24381/cds.239d815c, datalink (https://cds.climate.copernicus.eu/cdsapp#!/dataset/satellite-aerosol-properties?tab=form). For downloading the aforementioned MERIS data, following parameters were selected: Time aggregation (Monthly Average), Variable (Aerosol Optical Depth), Sensor on satellite (MERIS on ENVISAT), Algorithm (S4M (SeaWiFS algorithm for MERIS sensor)), year(2010) and Version (v7.0a). Additionally, the AERONET Level 2 AOD data for the 5 locations namely; Kanpur(26.513N, 80.232E), Gandhi College (25.871N, 84.128E), Nainital (29.359N, 79.458E), Pune (18.537N, 73.805E) and Jaipur(26.906N, 75.806E) was obtained from https://aeronet.gsfc.nasa.gov/cgi-bin/draw_map_display_aod_v3?long1=-180&long2=180&lat1=-90&lat2=90&multiplier=2&what_map=4&nachal=1&formatter=0&level=3&place_code=10&year=2010. The GEOS-Chem 3-D global model is freely available at https://geoschem.github.io/. For visualization, open-source software QGIS (Download: https://www.qgis.org/en/site/forusers/download.html) and Python programming code were used. The modeled data is available on https://data.mendeley.com/datasets/mh55488db3/1.

Acknowledgments

We thank the GEOS-Chem model community for making the data available. This work has been partly funded by the Deutsche Forschungsgemeinschaft (DFG, German Research Foundation) within the project "Arctic Amplification: Climate Relevant Atmospheric and Surface Processes, and Feedback Mechanisms (AC)^3" as Transregional Collaborative Research Center (TRR) 172, Project-ID 268020496. Usage of High-performance computing system cobra *Cobra, max planck computing and data facility* (n.d.) (https://www.mpcdf.mpg.de/services/supercomputing/cobra) is acknowledged.

References

Alpert, P., Shvainshtein, O., & Kishcha, P. (2012). AOD trends over megacities based on space monitoring using MODIS and MISR. *American Journal of Climate Change*, *01*(03), 117–131. Retrieved from https://doi.org/10.4236/ajcc.2012.13010 doi: 10.4236/ajcc.2012.13010

Andreae, M. O. (1993). The influence of tropical biomass burning on climate and the atmospheric environment. In *Biogeochemistry of global change* (pp. 113–150). Springer US. Retrieved from https://doi.org/10.1007/978-1-4615-2812-8_7 doi: 10.1007/978-1-4615-2812-8_7

Andreae, M. O., & Gelencsér, A. (2006, July). Black carbon or brown carbon? the nature of light-absorbing carbonaceous aerosols. *Atmospheric Chemistry and Physics*, *6*(10), 3131–3148. Retrieved from https://doi.org/10.5194/acp-6-3131-2006 doi: 10.5194/acp-6-3131-2006

Bey, I., Jacob, D. J., Yantosca, R. M., Logan, J. A., Field, B. D., Fiore, A. M., ... Schultz, M. G. (2001). Global modeling of tropospheric chemistry with assimilated meteorology: Model description and evaluation. *Journal of Geophysical Research: Atmospheres*, *106*(D19), 23073–23095.

Bikkina, S., Andersson, A., Kirillova, E. N., Holmstrand, H., Tiwari, S., Srivastava, A. K., ... Örjan Gustafsson (2019, February). Air quality in megacity delhi affected by countryside biomass burning. *Nature Sustainability*, *2*(3), 200–205. Retrieved from https://doi.org/10.1038/s41893-019-0219-0 doi: 10.1038/s41893-019-0219-0

Biswas, J., Pathak, B., Patadia, F., Bhuyan, P. K., Gogoi, M. M., & Babu, S. S. (2017, February). Satellite-retrieved direct radiative forcing of aerosols over north-east india and adjoining areas: climatology and impact assessment. *International Journal of Climatology*, *37*, 298–317. Retrieved from https://doi.org/10.1002/joc.5004 doi: 10.1002/joc.5004

Bouwman, A. F., Lee, D. S., Asman, W. A. H., Dentener, F. J., Hoek, K. W. V. D., & Olivier, J. G. J. (1997, December). A global high-resolution emission inventory for ammonia. *Global Biogeochemical Cycles*, *11*(4), 561–587. Retrieved from https://doi.org/10.1029/97gb02266 doi: 10.1029/97gb02266

Butt, E. W., Rap, A., Schmidt, A., Scott, C. E., Pringle, K. J., Reddington, C. L., ... Spracklen, D. V. (2016, January). The impact of residential combustion emissions on atmospheric aerosol, human health, and climate. *Atmospheric Chemistry and Physics*, *16*(2), 873–905. Retrieved from https://doi.org/10.5194/acp-16-873-2016 doi: 10.5194/acp-16-873-2016

Chawala, P., R, S. P., & SM, S. N. (2023, March). Climatology and landscape determinants of AOD, SO2 and NO2 over indo-gangetic plain. *Environmental Research*, *220*, 115125. Retrieved from https://doi.org/10.1016/j.envres.2022.115125 doi: 10.1016/j.envres.2022.115125

Chin, M., Ginoux, P., Kinne, S., Torres, O., Holben, B. N., Duncan, B. N., ... Nakajima, T. (2002, February). Tropospheric aerosol optical thickness from the GOCART model and comparisons with satellite and sun photometer measurements. *Journal of the Atmospheric Sciences*, *59*(3), 461–483. Retrieved from https://doi.org/10.1175/1520-0469(2002)059<0461:taotft>2.0.co;2 doi: 10.1175/1520-0469(2002)059⟨0461:taotft⟩2.0.co;2

Chowdhury, S., Dey, S., & Smith, K. R. (2018, January). Ambient PM2.5 exposure and expected premature mortality to 2100 in india under climate change scenarios. *Nature Communications*, *9*(1). Retrieved from https://doi.org/10.1038/s41467-017-02755-y doi: 10.1038/s41467-017-02755-y

Cobra, max planck computing and data facility. (n.d.). Retrieved from https://www.mpcdf.mpg.de/services/supercomputing/cobra

Cowan, T., & Cai, W. (2011, June). The impact of asian and non-asian anthropogenic aerosols on 20th century asian summer monsoon. *Geophysical Research Letters*, *38*(11), n/a–n/a. Retrieved from https://doi.org/10.1029/2011gl047268 doi: 10.1029/2011gl047268

David, L. M., Ravishankara, A. R., Kodros, J. K., Pierce, J. R., Venkataraman, C., & Sadavarte, P. (2019). Premature mortality due to pm2.5 over india: Effect of atmospheric transport and anthropogenic emissions. *GeoHealth*, *3*(1), 2-10. Retrieved from https://agupubs.onlinelibrary.wiley.com/doi/abs/10.1029/2018GH000169 doi: https://doi.org/10.1029/2018GH000169

David, L. M., Ravishankara, A. R., Kodros, J. K., Venkataraman, C., Sadavarte, P., Pierce, J. R., ... Millet, D. B. (2018). Aerosol optical depth over india. *Journal of Geophysical Research: Atmospheres*, *123*(7), 3688-3703. Retrieved from https://agupubs.onlinelibrary.wiley.com/doi/abs/10.1002/2017JD027719 doi: https://doi.org/10.1002/2017JD027719

Dey, S., Tripathi, S. N., Singh, R. P., & Holben, B. N. (2004). Influence of dust storms on the aerosol optical properties over the indo-gangetic basin. *Journal of Geophysical Research: Atmospheres*, *109*(D20). Retrieved from https://agupubs.onlinelibrary.wiley.com/doi/abs/10.1029/2004JD004924 doi: https://doi.org/10.1029/2004JD004924

Dutta, M., & Chatterjee, A. (2021, June). Assessment of the relative influences of long-range transport, fossil fuel and biomass burning from aerosol pollution under restricted anthropogenic emissions: A national scenario in india. *Atmospheric Environment*, *255*, 118423. Retrieved from https://doi.org/10.1016/j.atmosenv.2021.118423 doi: 10.1016/j.atmosenv.2021.118423

FLANNIGAN, M., STOCKS, B., TURETSKY, M., & WOTTON, M. (2009, March). Impacts of climate change on fire activity and fire management in the circumboreal forest. *Global Change Biology*, *15*(3), 549–560. Retrieved from https://doi.org/10.1111/j.1365-2486.2008.01660.x doi: 10.1111/j.1365-2486.2008.01660.x

Galanter, M., Levy II, H., & Carmichael, G. R. (2000). Impacts of biomass burning on tropospheric co, no x , and o3. *Journal of Geophysical Research: Atmospheres*, *105*(D5), 6633-6653. Retrieved from https://agupubs.onlinelibrary.wiley.com/doi/abs/10.1029/1999JD901113 doi: https://doi.org/10.1029/1999JD901113

Group, G. M. W., et al. (2018). *Burden of disease attributable to major air pollution sources in india. special report 21. boston, ma: Health effects institute [www document]. published 2018.*

Guenther, A., Karl, T., Harley, P., Wiedinmyer, C., Palmer, P. I., & Geron, C. (2006, August). Estimates of global terrestrial isoprene emissions using MEGAN (model of emissions of gases and aerosols from nature). *Atmospheric Chemistry and Physics*, *6*(11), 3181–3210. Retrieved from https://doi.org/10.5194/acp-6-3181-2006 doi: 10.5194/acp-6-3181-2006

Gulia, S., Shukla, N., Padhi, L., Bosu, P., Goyal, S., & Kumar, R. (2022). Evolution of air pollution management policies and related research in india. *Environmental Challenges*, *6*, 100431. Retrieved from https://www.sciencedirect.com/science/article/pii/S2667010021004054 doi: https://doi.org/10.1016/j.envc.2021.100431

Gunthe, S. S., Liu, P., Panda, U., Raj, S. S., Sharma, A., Darbyshire, E., … Coe, H. (2021, January). Enhanced aerosol particle growth sustained by high continental chlorine emission in india. *Nature Geoscience*, *14*(2), 77–84. Retrieved from https://doi.org/10.1038/s41561-020-00677-x doi: 10.1038/s41561-020-00677-x

Haywood, J. (2021). Atmospheric aerosols and their role in climate change. In *Climate change* (pp. 645–659). Elsevier. Retrieved from https://doi.org/10.1016/b978-0-12-821575-3.00030-x doi: 10.1016/b978-0-12-821575-3.00030-x

Holben, B., Eck, T., Slutsker, I., Tanré, D., Buis, J., Setzer, A., … Smirnov, A. (1998, October). AERONET—a federated instrument network and data archive for aerosol characterization. *Remote Sensing of Environment*, *66*(1), 1–16. Retrieved from https://doi.org/10.1016/s0034-4257(98)00031-5 doi: 10.1016/s0034-4257(98)00031-5

Intergovernmental Panel on Climate Change. (2014). Climate Change 2014: Synthesis Report. In Core Writing Team and Pachauri, R.K. and Meyer, L.A. (Ed.), *Climate Change 2014: Synthesis Report* (p. 93-129). Cambridge, UK: Cambridge University Press.

Jin, Q., Wei, J., Pu, B., Yang, Z.-L., & Parajuli, S. P. (2018, September). High summertime aerosol loadings over the arabian sea and their transport pathways. *Journal of Geophysical Research: Atmospheres*, *123*(18). Retrieved from https://doi.org/10.1029/2018jd028588 doi: 10.1029/2018jd028588

Keywood, M., Kanakidou, M., Stohl, A., Dentener, F., Grassi, G., Meyer, C. P., … Burrows, J. (2011, October). Fire in the air: Biomass burning impacts in a changing climate. *Critical Reviews in Environmental Science and Technology*, *43*(1), 40–83. Retrieved from https://

doi.org/10.1080/10643389.2011.604248 doi: 10.1080/10643389.2011.604248

Kokhanovsky, A., Breon, F.-M., Cacciari, A., Carboni, E., Diner, D., Nicolantonio, W. D., ... von Hoyningen-Huene, W. (2007, September). Aerosol remote sensing over land: A comparison of satellite retrievals using different algorithms and instruments. *Atmospheric Research*, *85*(3-4), 372–394. Retrieved from https://doi.org/10.1016/j.atmosres.2007.02.008 doi: 10.1016/j.atmosres.2007.02.008

Kumar, B., Chakraborty, A., Tripathi, S. N., & Bhattu, D. (2016). Highly time resolved chemical characterization of submicron organic aerosols at a polluted urban location. *Environ. Sci.: Processes Impacts*, *18*, 1285-1296. Retrieved from http://dx.doi.org/10.1039/C6EM00392C doi: 10.1039/C6EM00392C

Kumar, M., Parmar, K., Kumar, D., Mhawish, A., Broday, D., Mall, R., & Banerjee, T. (2018, May). Long-term aerosol climatology over indo-gangetic plain: Trend, prediction and potential source fields. *Atmospheric Environment*, *180*, 37–50. Retrieved from https://doi.org/10.1016/j.atmosenv.2018.02.027 doi: 10.1016/j.atmosenv.2018.02.027

Kumar, P., Beig, G., Sahu, S., Yadav, R., Maji, S., Singh, V., & Bamniya, B. (2023, June). Development of a high-resolution emissions inventory of carbonaceous particulate matters and their growth during 2011–2018 over india. *Atmospheric Environment*, *303*, 119750. Retrieved from https://doi.org/10.1016/j.atmosenv.2023.119750 doi: 10.1016/j.atmosenv.2023.119750

Kumar, R., Naja, M., Satheesh, S. K., Ojha, N., Joshi, H., Sarangi, T., ... Venkataramani, S. (2011, October). Influences of the springtime northern indian biomass burning over the central himalayas. *Journal of Geophysical Research*, *116*(D19). Retrieved from https://doi.org/10.1029/2010jd015509 doi: 10.1029/2010jd015509

Lee, H.-H., Bar-Or, R. Z., & Wang, C. (2017, January). Biomass burning aerosols and the low-visibility events in southeast asia. *Atmospheric Chemistry and Physics*, *17*(2), 965–980. Retrieved from https://doi.org/10.5194/acp-17-965-2017 doi: 10.5194/acp-17-965-2017

Levy, H., Horowitz, L. W., Schwarzkopf, M. D., Ming, Y., Golaz, J.-C., Naik, V., & Ramaswamy, V. (2013, May). The roles of aerosol direct and indirect effects in past and future climate change. *Journal of Geophysical Research: Atmospheres*, *118*(10), 4521–4532. Retrieved from https://doi.org/10.1002/jgrd.50192 doi: 10.1002/jgrd.50192

Li, K., Liao, H., Zhu, J., & Moch, J. M. (2016). Implications of rcp emissions on future pm2.5 air quality and direct radiative forcing over china. *Journal of Geophysical Research: Atmospheres*, *121*(21), 12,985-13,008. Retrieved from https://agupubs.onlinelibrary.wiley.com/doi/abs/10.1002/2016JD025623 doi: https://doi.org/10.1002/2016JD025623

Liu, D., He, C., Schwarz, J. P., & Wang, X. (2020, October). Lifecycle of light-absorbing carbonaceous aerosols in the atmosphere. *npj Climate and Atmospheric Science*, *3*(1). Retrieved from https://doi.org/10.1038/s41612-020-00145-8 doi: 10.1038/s41612-020-00145-8

Lodhi, N. K., Beegum, S. N., Singh, S., & Kumar, K. (2013, February). Aerosol climatology at delhi in the western indo-gangetic plain: Microphysics, long-term trends, and source strengths. *Journal of Geophysical Research: Atmospheres*, *118*(3), 1361–1375. Retrieved from https://doi.org/10.1002/jgrd.50165 doi: 10.1002/jgrd.50165

Lu, Z., Zhang, Q., & Streets, D. G. (2011, September). Sulfur dioxide and primary carbonaceous aerosol emissions in china and india, 1996–2010. *Atmospheric Chemistry and Physics*, *11*(18), 9839–9864. Retrieved from https://doi.org/10.5194/acp-11-9839-2011 doi: 10.5194/acp-11-9839-2011

Mangla, R., J, I., & S.S., C. (2020, August). Inter-comparison of multi-satellites and aeronet AOD over indian region. *Atmospheric Research*, *240*, 104950. Retrieved from https://doi.org/10.1016/j.atmosres.2020.104950 doi: 10.1016/j.atmosres.2020.104950

Mei, L., Rozanov, V., Vountas, M., Burrows, J. P., Levy, R. C., & Lotz, W. (2017, August). Retrieval of aerosol optical properties using MERIS observations: Algorithm and some first results. *Remote Sensing of Environment*, *197*, 125–140. Retrieved from https://doi.org/10.1016/j.rse.2016.11.015 doi: 10.1016/j.rse.2016.11.015

Mei, L., Vountas, M., Gómez-Chova, L., Rozanov, V., Jäger, M., Lotz, W., ... Hollmann, R. (2017, August). A cloud masking algorithm for the XBAER aerosol retrieval using MERIS data. *Remote Sensing of Environment*, *197*, 141–160. Retrieved from https://doi.org/10.1016/j.rse.2016.11.016 doi: 10.1016/j.rse.2016.11.016

Mhawish, A., Sorek-Hamer, M., Chatfield, R., Banerjee, T., Bilal, M., Kumar, M., ... Kalashnikova, O. (2021, June). Aerosol characteristics from earth observation systems: A comprehensive investigation over south asia (2000–2019). *Remote Sensing of Environment*, *259*, 112410. Retrieved from https://doi.org/10.1016/j.rse.2021.112410 doi: 10.1016/j.rse.2021.112410

Misra, A., Gaur, A., Bhattu, D., Ghosh, S., Dwivedi, A. K., Dalai, R., ... Tripathi, S. N. (2014, November). An overview of the physico-chemical characteristics of dust at kanpur in the central indo-gangetic basin. *Atmospheric Environment*, *97*, 386–396. Retrieved from https://doi.org/10.1016/j.atmosenv.2014.08.043 doi: 10.1016/j.atmosenv.2014.08.043

Mitra, A., & Sharma, C. (2002, December). Indian aerosols: present status. *Chemosphere*, *49*(9), 1175–1190. Retrieved from https://doi.org/10.1016/s0045-6535(02)00247-3 doi: 10.1016/s0045-6535(02)00247-3

Mogno, C., Palmer, P. I., Knote, C., Yao, F., & Wallington, T. J. (2021, July). Seasonal distribution and drivers of surface fine particulate matter and organic aerosol over the indo-gangetic plain. *Atmospheric Chemistry and Physics*, *21*(14), 10881–10909. Retrieved from https://doi.org/10.5194/acp-21-10881-2021 doi: 10.5194/acp-21-10881-2021

Murphy, D. M., Froyd, K. D., Bian, H., Brock, C. A., Dibb, J. E., DiGangi, J. P., ... Yu, P. (2019, April). The distribution of sea-salt aerosol in the global troposphere. *Atmospheric Chemistry and Physics*, *19*(6), 4093–4104. Retrieved from https://doi.org/10.5194/acp-19-4093-2019 doi: 10.5194/acp-19-4093-2019

Murray, L. T., Jacob, D. J., Logan, J. A., Hudman, R. C., & Koshak, W. J. (2012, October). Optimized regional and interannual variability of lightning in a global chemical transport model constrained by LIS/OTD satellite data. *Journal of Geophysical Research: Atmospheres*, *117*(D20). Retrieved from https://doi.org/10.1029/2012jd017934 doi: 10.1029/2012jd017934

Nandini, G., Vinoj, V., & Pandey, S. K. (2022, March). Arabian sea aerosol-indian summer monsoon rainfall relationship and its modulation by el-nino southern oscillation. *npj Climate and Atmospheric Science*, *5*(1). Retrieved from https://doi.org/10.1038/s41612-022-00244-8 doi: 10.1038/s41612-022-00244-8

Ojha, N., Sharma, A., Kumar, M., Girach, I., Ansari, T. U., Sharma, S. K., ... Gunthe, S. S. (2020, April). On the widespread enhancement in fine particulate matter across the indo-gangetic plain towards winter. *Scientific Reports*, *10*(1). Retrieved from https://doi.org/10.1038/s41598-020-62710-8 doi: 10.1038/s41598-020-62710-8

Park, R. J., Jacob, D. J., Chin, M., & Martin, R. V. (2003). Sources of carbonaceous aerosols over the united states and implications for natural visibility. *Journal of Geophysical Research: Atmospheres*, *108*(D12).

Perera, F. (2017, December). Pollution from fossil-fuel combustion is the leading environmental threat to global pediatric health and equity: Solutions exist. *Int. J. Environ. Res. Public Health*, *15*(1), 16.

Provençal, S., Kishcha, P., da Silva, A. M., Elhacham, E., & Alpert, P. (2017, June). AOD distributions and trends of major aerosol species over a selection of the world's most populated cities based on the 1st version of NASA's MERRA aerosol reanalysis. *Urban Climate*, *20*, 168–191. Retrieved from https://doi.org/10.1016/j.uclim.2017.04.001 doi: 10.1016/j.uclim.2017.04.001

Rajeev, K., Ramanathan, V., & Meywerk, J. (2000, January). Regional aerosol distribution and its long-range transport over the indian ocean. *Journal of Geophysical Research: Atmospheres*, *105*(D2), 2029–2043. Retrieved from https://doi.org/10.1029/1999jd900414 doi: 10.1029/1999jd900414

Rajesh, T. A., & Ramachandran, S. (2017, February). Characteristics and source apportionment of black carbon aerosols over an urban site. *Environmental Science and Pollution Research*, *24*(9), 8411–8424. Retrieved from https://doi.org/10.1007/s11356-017-8453-3 doi: 10.1007/s11356-017-8453-3

Ramachandran, S., & Cherian, R. (2008, April). Regional and seasonal variations in aerosol optical characteristics and their frequency distributions over india during 2001–2005. *Journal of Geophysical Research*, *113*(D8). Retrieved from https://doi.org/10.1029/2007jd008560 doi: 10.1029/2007jd008560

Ramachandran, S., Kedia, S., & Srivastava, R. (2012, March). Aerosol optical depth trends over different regions of india. *Atmospheric Environment*, *49*, 338–347. Retrieved from https://doi.org/10.1016/j.atmosenv.2011.11.017 doi: 10.1016/j.atmosenv.2011.11.017

Rawat, P., Sarkar, S., Jia, S., Khillare, P. S., & Sharma, B. (2019, July). Regional sulfate drives long-term rise in AOD over megacity kolkata, india. *Atmospheric Environment*, *209*, 167–181. Retrieved from https://doi.org/10.1016/j.atmosenv.2019.04.031 doi: 10.1016/j.atmosenv.2019.04.031

Reisen, F., Meyer, C. M., & Keywood, M. D. (2013, March). Impact of biomass burning sources on seasonal aerosol air quality. *Atmospheric Environment*, *67*, 437–447. Retrieved from https://doi.org/10.1016/j.atmosenv.2012.11.004 doi: 10.1016/j.atmosenv.2012.11.004

Saha, U., Siingh, D., Kamra, A., Galanaki, E., Maitra, A., Singh, R., ... Singh, R. (2017, January). On the association of lightning activity and projected change in climate over the indian subcontinent. *Atmospheric Research*, *183*, 173–190. Retrieved from https://doi.org/10.1016/j.atmosres.2016.09.001 doi: 10.1016/j.atmosres.2016.09.001

Sarangi, C., Kanawade, V. P., Tripathi, S. N., Thomas, A., & Ganguly, D. (2018, September). Aerosol-induced intensification of cooling effect of clouds during indian summer monsoon. *Nature Communications*, *9*(1). Retrieved from https://doi.org/10.1038/s41467-018-06015-5 doi: 10.1038/s41467-018-06015-5

Sauvage, B., Martin, R. V., van Donkelaar, A., Liu, X., Chance, K., Jaeglé, L., ... Fu, T.-M. (2007, February). Remote sensed and in situ constraints on processes affecting tropical tropospheric ozone. *Atmospheric Chemistry and Physics*, *7*(3), 815–838. Retrieved from https://doi.org/10.5194/acp-7-815-2007 doi: 10.5194/acp-7-815-2007

Seinfeld, J. H., & Pandis, S. N. (2016). *Atmospheric chemistry and physics: From air pollution to climate change*. Wiley.

Sharma, A. R., Kharol, S. K., Badarinath, K. V. S., & Singh, D. (2010). Impact of agriculture crop residue burning on atmospheric aerosol loading –a study over punjab state, india. *Annales Geophysicae*, *28*(2), 367–379. Retrieved from https://angeo.copernicus.org/articles/28/367/2010/ doi: 10.5194/angeo-28-367-2010

Shekar Reddy, M., & Venkataraman, C. (2000). Atmospheric optical and radiative effects of anthropogenic aerosol constituents from india. *Atmospheric Environment*, *34*(26), 4511-4523. Retrieved from https://www.sciencedirect.com/science/article/pii/S1352231000001059 doi: https://doi.org/10.1016/S1352-2310(00)00105-9

Shiraiwa, M., Ueda, K., Pozzer, A., Lammel, G., Kampf, C. J., Fushimi, A., ... Sato, K. (2017, November). Aerosol health effects from molecular to global scales. *Environmental Science & Technology*, *51*(23), 13545–13567. Retrieved from https://doi.org/10.1021/acs.est.7b04417 doi: 10.1021/acs.est.7b04417

Shukla, K., Sarangi, C., Attada, R., & Kumar, P. (2022). Characteristic dissimilarities during high aerosol loading days between western and eastern indo-gangetic plain. *Atmospheric Environment*, *269*, 118837. Retrieved from https://www.sciencedirect.com/science/article/pii/S1352231021006592 doi: https://doi.org/10.1016/j.atmosenv.2021.118837

Singh, A., Rastogi, N., Patel, A., & Singh, D. (2016, December). Seasonality in size-segregated ionic composition of ambient particulate pollutants over the indo-gangetic plain: Source apportionment using PMF. *Environmental Pollution*, *219*, 906–915. Retrieved from https://doi.org/10.1016/j.envpol.2016.09.010 doi: 10.1016/j.envpol.2016.09.010

Song, Z., Fu, D., Zhang, X., Wu, Y., Xia, X., He, J., ... Che, H. (2018, October). Diurnal and seasonal variability of PM2.5 and AOD in north china plain: Comparison of MERRA-2 products and ground measurements. *Atmospheric Environment*, *191*, 70–78. Retrieved from https://doi.org/10.1016/j.atmosenv.2018.08.012 doi: 10.1016/j.atmosenv.2018.08.012

Srivastava, A., & Saran, S. (2017, May). Comprehensive study on AOD trends over the indian subcontinent: a statistical approach. *International Journal of Remote Sensing*, *38*(18), 5127–5149. Retrieved from https://doi.org/10.1080/01431161.2017.1323284 doi: 10.1080/01431161.2017.1323284

Streets, D. G., Yarber, K. F., Woo, J.-H., & Carmichael, G. R. (2003). Biomass burning in asia: Annual and seasonal estimates and atmospheric emissions. *Global Biogeochemical Cycles*, *17*(4). Retrieved from https://agupubs.onlinelibrary.wiley.com/doi/abs/10.1029/2003GB002040 doi: https://doi.org/10.1029/2003GB002040

Taylor, D. (2009, December). Biomass burning, humans and climate change in southeast asia. *Biodiversity and Conservation*, *19*(4), 1025–1042. Retrieved from https://doi.org/10.1007/s10531-009-9756-6 doi: 10.1007/s10531-009-9756-6

Thiemens, M., & Shaheen, R. (2014). Mass-independent isotopic composition of terrestrial and extraterrestrial materials. In *Treatise on geochemistry* (pp. 151–177). Elsevier. Retrieved from https://doi.org/10.1016/b978-0-08-095975-7.00406-x doi: 10.1016/b978-0-08-095975-7.00406-x

Tripathi, S. N., Tare, V., Chinnam, N., Srivastava, A. K., Dey, S., Agarwal, A., ... Lal, S. (2006). Measurements of atmospheric parameters during indian space research organization geosphere biosphere programme land campaign ii at a typical location in the ganga basin: 1. physical and optical properties. *Journal of Geophysical Research: Atmospheres*, *111*(D23). Retrieved from https://agupubs.onlinelibrary.wiley.com/doi/abs/10.1029/2006JD007278 doi: https://doi.org/10.1029/2006JD007278

Tyagi, B., Choudhury, G., Vissa, N. K., Singh, J., & Tesche, M. (2021, February). Changing air pollution scenario during COVID-19: Redefining the hotspot regions over india. *Environmental Pollution*, *271*, 116354. Retrieved from https://doi.org/10.1016/j.envpol.2020.116354 doi: 10.1016/j.envpol.2020.116354

van Vuuren, D. P., Edmonds, J., Kainuma, M., Riahi, K., Thomson, A., Hibbard, K., ... Rose, S. K. (2011, August). The representative concentration pathways: an overview. *Climatic Change*, *109*(1-2), 5–31. Retrieved from https://doi.org/10.1007/s10584-011-0148-z doi: 10.1007/s10584-011-0148-z

Venkataraman, C., Habib, G., Kadamba, D., Shrivastava, M., Leon, J.-F., Crouzille, B., ... Streets, D. G. (2006, June). Emissions from open biomass burning in india: Integrating the inventory approach with high-resolution moderate resolution imaging spectroradiometer (MODIS) active-fire and land cover data. *Global Biogeochemical Cycles*, *20*(2), n/a–n/a. Retrieved from https://doi.org/10.1029/2005gb002547 doi: 10.1029/2005gb002547

Xie, M., Hays, M. D., & Holder, A. L. (2017, August). Light-absorbing organic carbon from prescribed and laboratory biomass burning and gasoline vehicle emissions. *Scientific Reports*, *7*(1). Retrieved from https://doi.org/10.1038/s41598-017-06981-8 doi: 10.1038/s41598-017-06981-8

Yadav, S., Tripathi, S. N., & Rupakheti, M. (2022, April). Current status of source apportionment of ambient aerosols in india. *Atmospheric Environment*, *274*, 118987. Retrieved from https://doi.org/10.1016/j.atmosenv.2022.118987 doi: 10.1016/j.atmosenv.2022.118987

Yang, Y., Ruan, Z., Wang, X., Yang, Y., Mason, T. G., Lin, H., & Tian, L. (2019, April). Short-term and long-term exposures to fine particulate matter constituents and health: A systematic review and meta-analysis. *Environmental Pollution*, *247*, 874–882. Retrieved from https://doi.org/10.1016/j.envpol.2018.12.060 doi: 10.1016/j.envpol.2018.12.060

Yienger, J. J., & Levy II, H. (1995). Empirical model of global soil-biogenic no_X emissions. *Journal of Geophysical Research: Atmospheres*, *100*(D6), 11447-11464. Retrieved from https://agupubs.onlinelibrary.wiley.com/doi/abs/10.1029/95JD00370 doi: https://doi.org/10.1029/95JD00370

Figure 1.

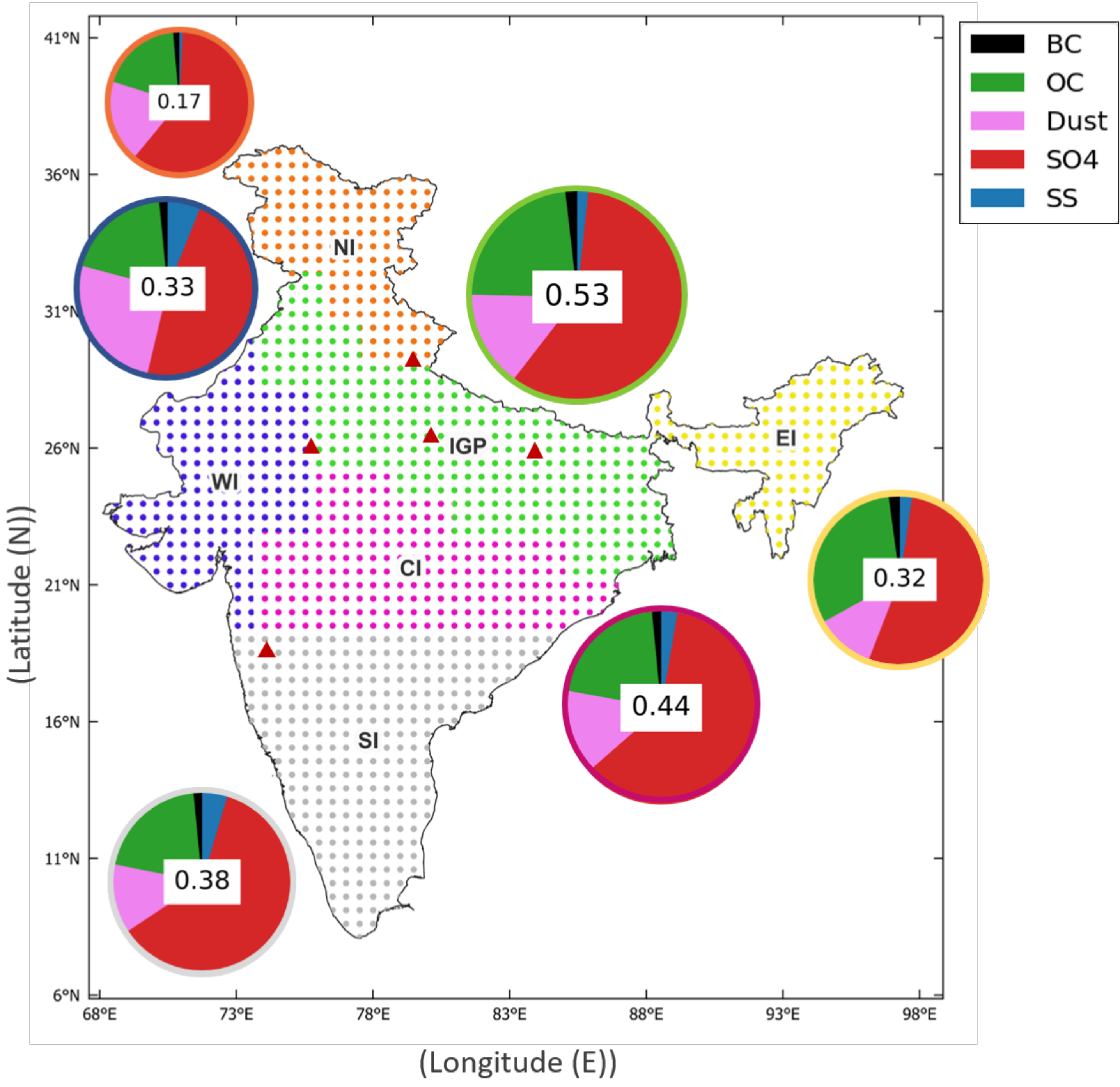

BC
OC
Dust
SO4
SS
0.17
0.33
0.53
0.32
0.44
0.38
NI
IGP
WI
CI
EI
SI
41°N
36°N
31°N
26°N
21°N
16°N
11°N
6°N
68°E
73°E
78°E
83°E
88°E
93°E
98°E
(Latitude (N))
(Longitude (E))

Figure 2.

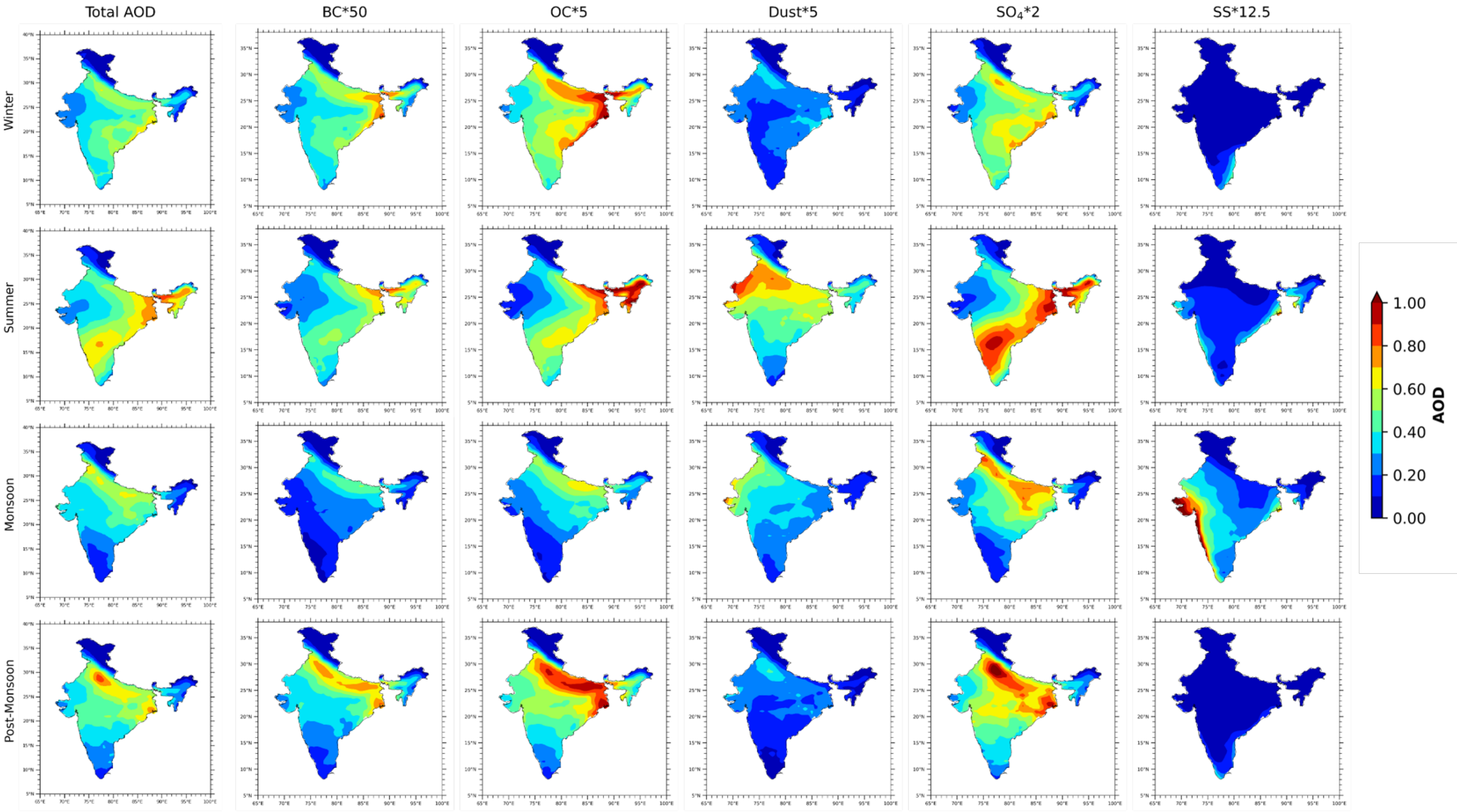
Total AOD
BC*50
OC*5
Dust*5
SO_4*2
SS*12.5
Winter
Summer
Monsoon
Post-Monsoon
AOD
1.00
0.80
0.60
0.40
0.20
0.00

Figure 3.

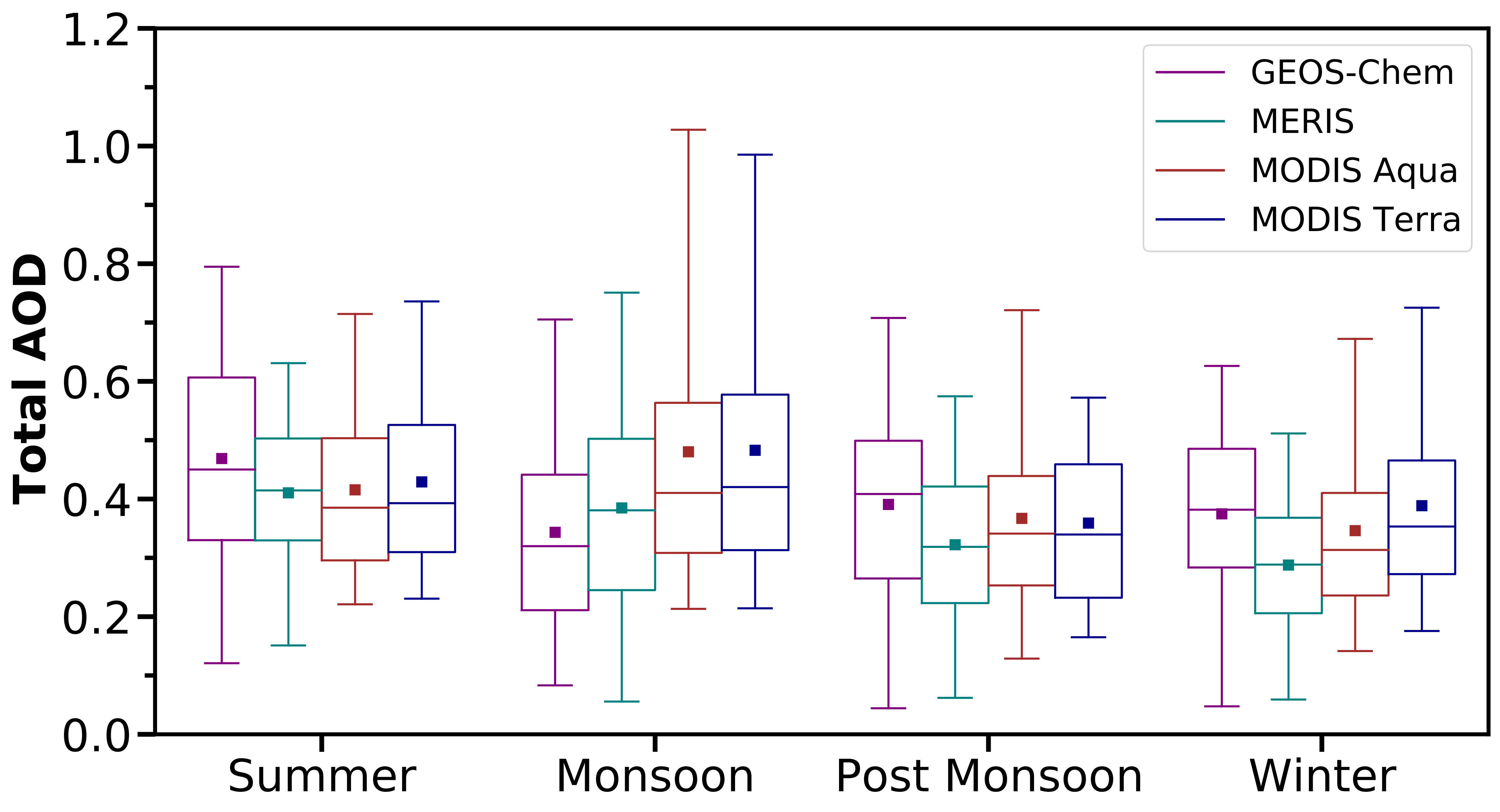

1.2
1.0
0.8
0.6
0.4
0.2
0.0
Total AOD
GEOS-Chem
MERIS
MODIS Aqua
MODIS Terra
Summer
Monsoon
Post Monsoon
Winter

Figure 4.

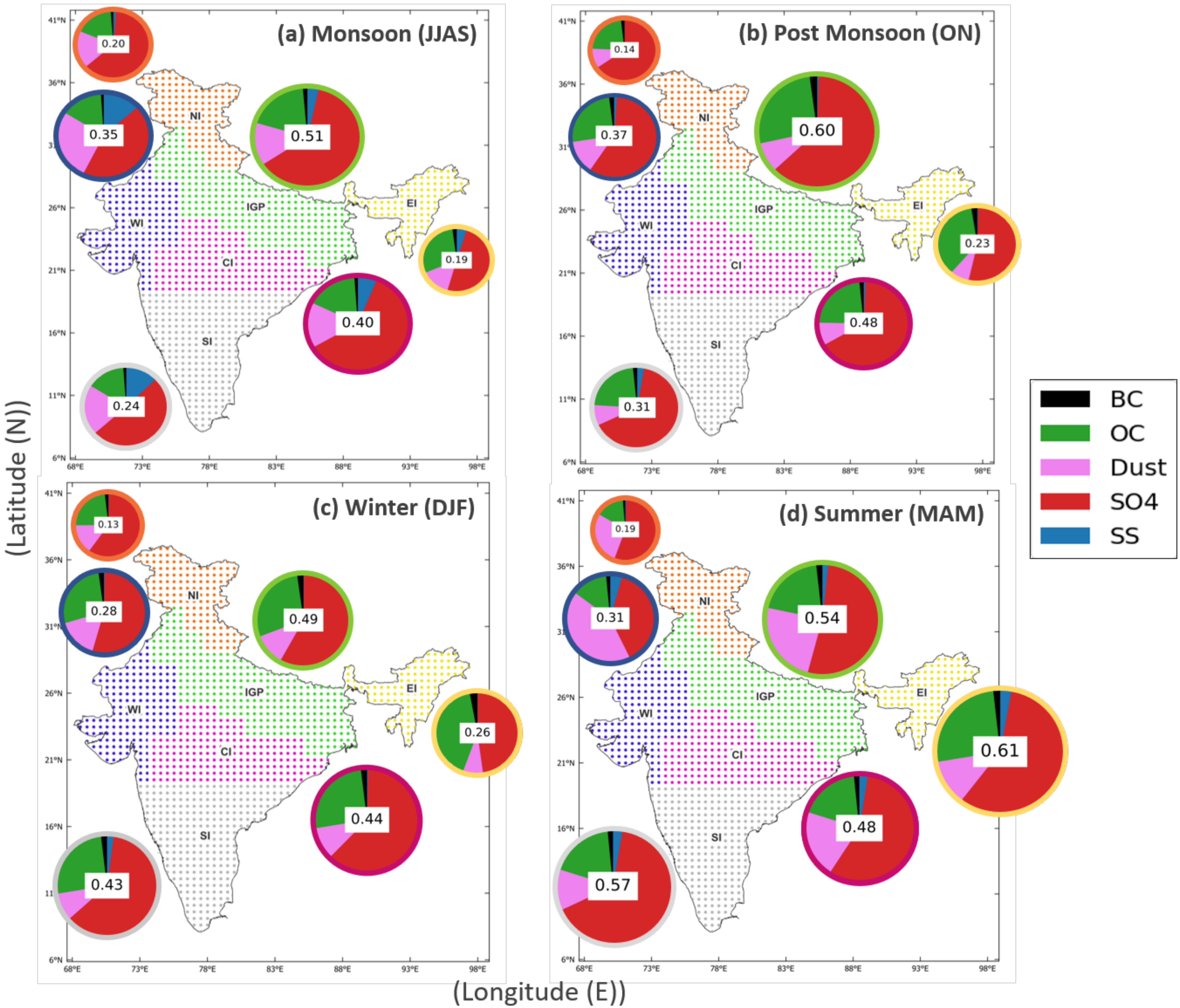
(a) Monsoon (JJAS)
(b) Post Monsoon (ON)
(c) Winter (DJF)
(d) Summer (MAM)
NI
IGP
WI
CI
EI
SI
0.20
0.35
0.51
0.19
0.40
0.24
0.14
0.37
0.60
0.23
0.48
0.31
0.13
0.28
0.49
0.26
0.44
0.43
0.19
0.31
0.54
0.61
0.48
0.57
BC
OC
Dust
SO4
SS
(Latitude (N))
(Longitude (E))

Figure 5.

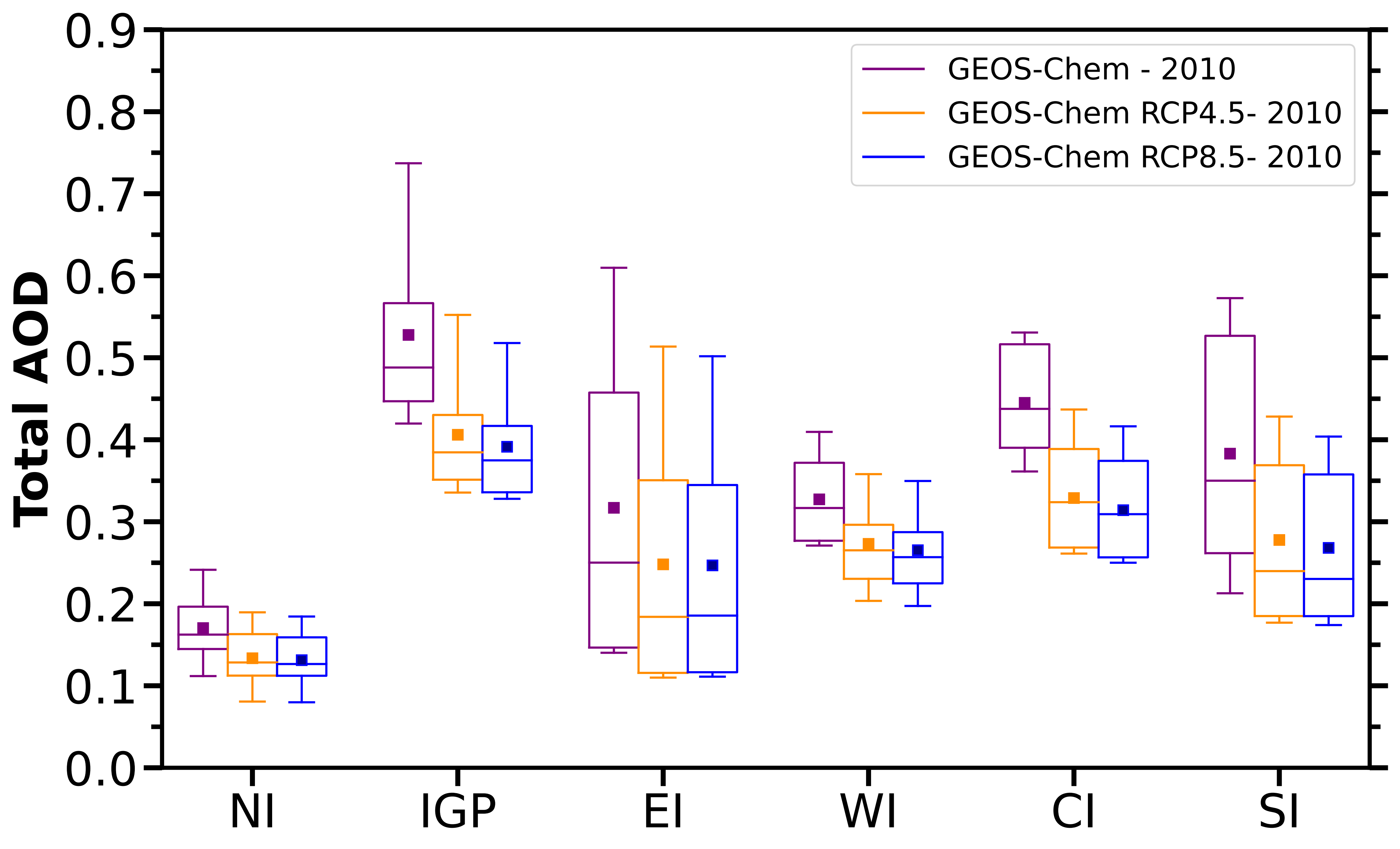
Total AOD
0.0
0.1
0.2
0.3
0.4
0.5
0.6
0.7
0.8
0.9
NI
IGP
EI
WI
CI
SI
GEOS-Chem - 2010
GEOS-Chem RCP4.5- 2010
GEOS-Chem RCP8.5- 2010

Figure 6.

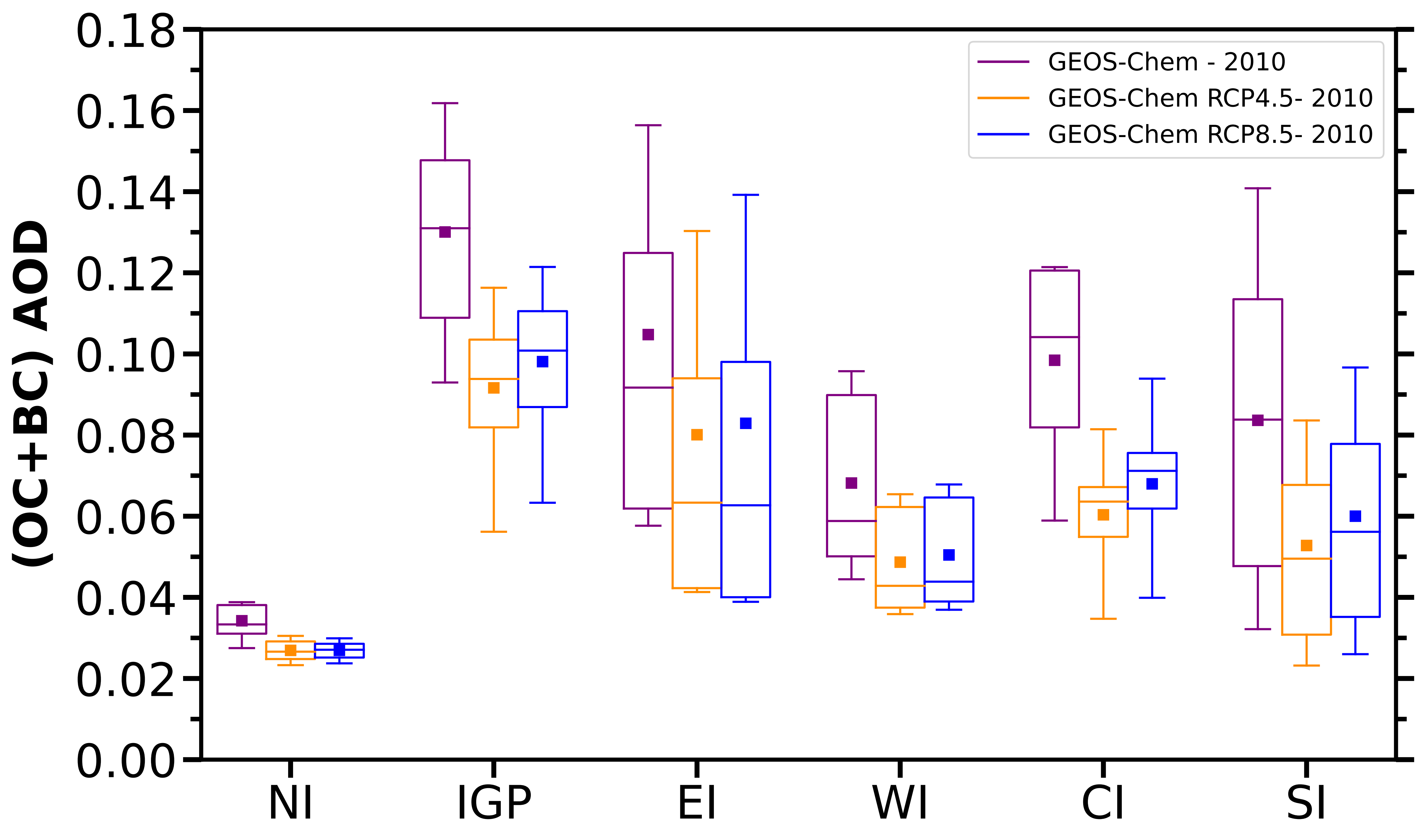

GEOS-Chem - 2010
GEOS-Chem RCP4.5- 2010
GEOS-Chem RCP8.5- 2010
(OC+BC) AOD
0.18
0.16
0.14
0.12
0.10
0.08
0.06
0.04
0.02
0.00
NI
IGP
EI
WI
CI
SI

Figure 7.

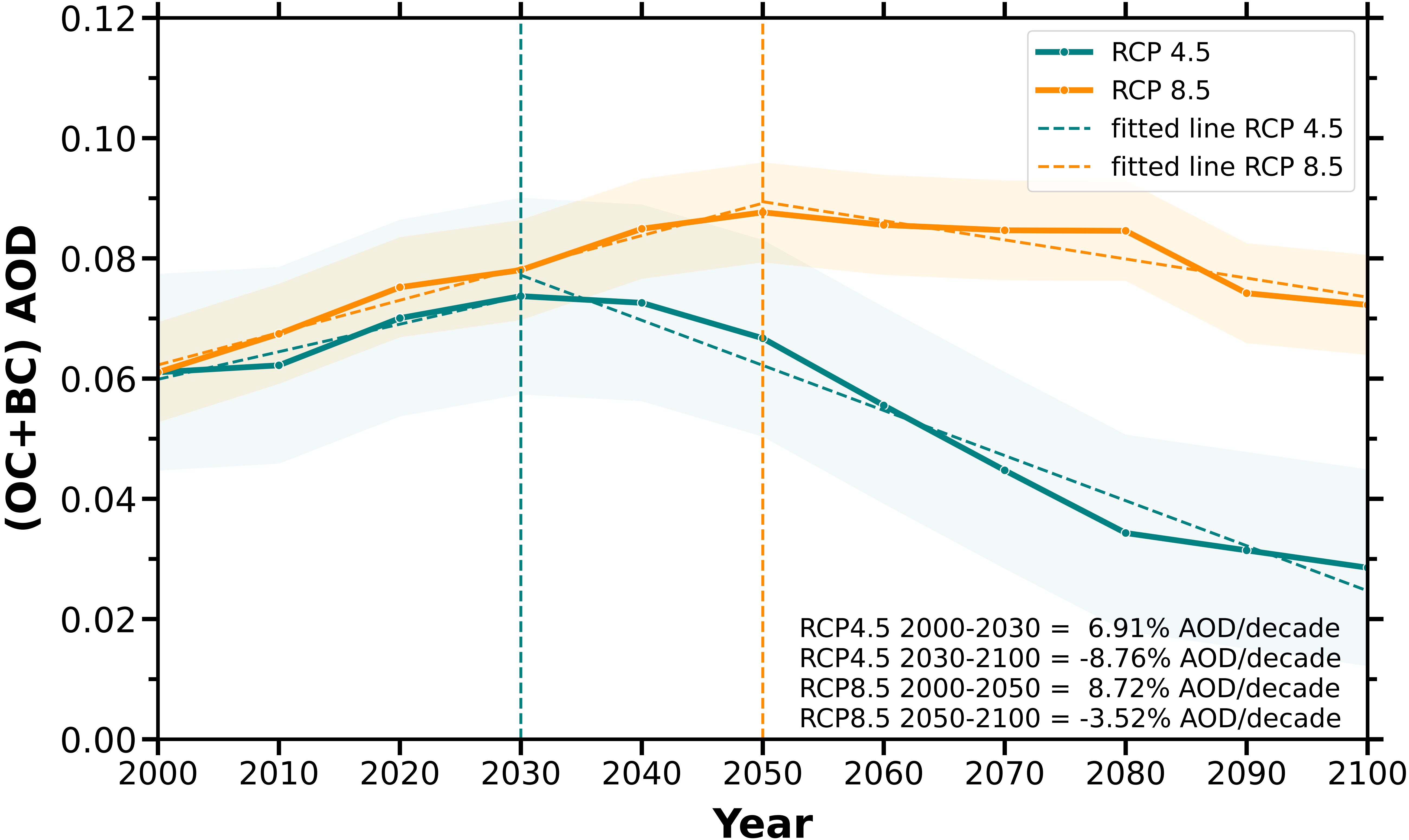

RCP 4.5
RCP 8.5
fitted line RCP 4.5
fitted line RCP 8.5
RCP4.5 2000-2030 = 6.91% AOD/decade
RCP4.5 2030-2100 = -8.76% AOD/decade
RCP8.5 2000-2050 = 8.72% AOD/decade
RCP8.5 2050-2100 = -3.52% AOD/decade
(OC+BC) AOD
Year
0.00
0.02
0.04
0.06
0.08
0.10
0.12
2000
2010
2020
2030
2040
2050
2060
2070
2080
2090
2100

Figure 8.

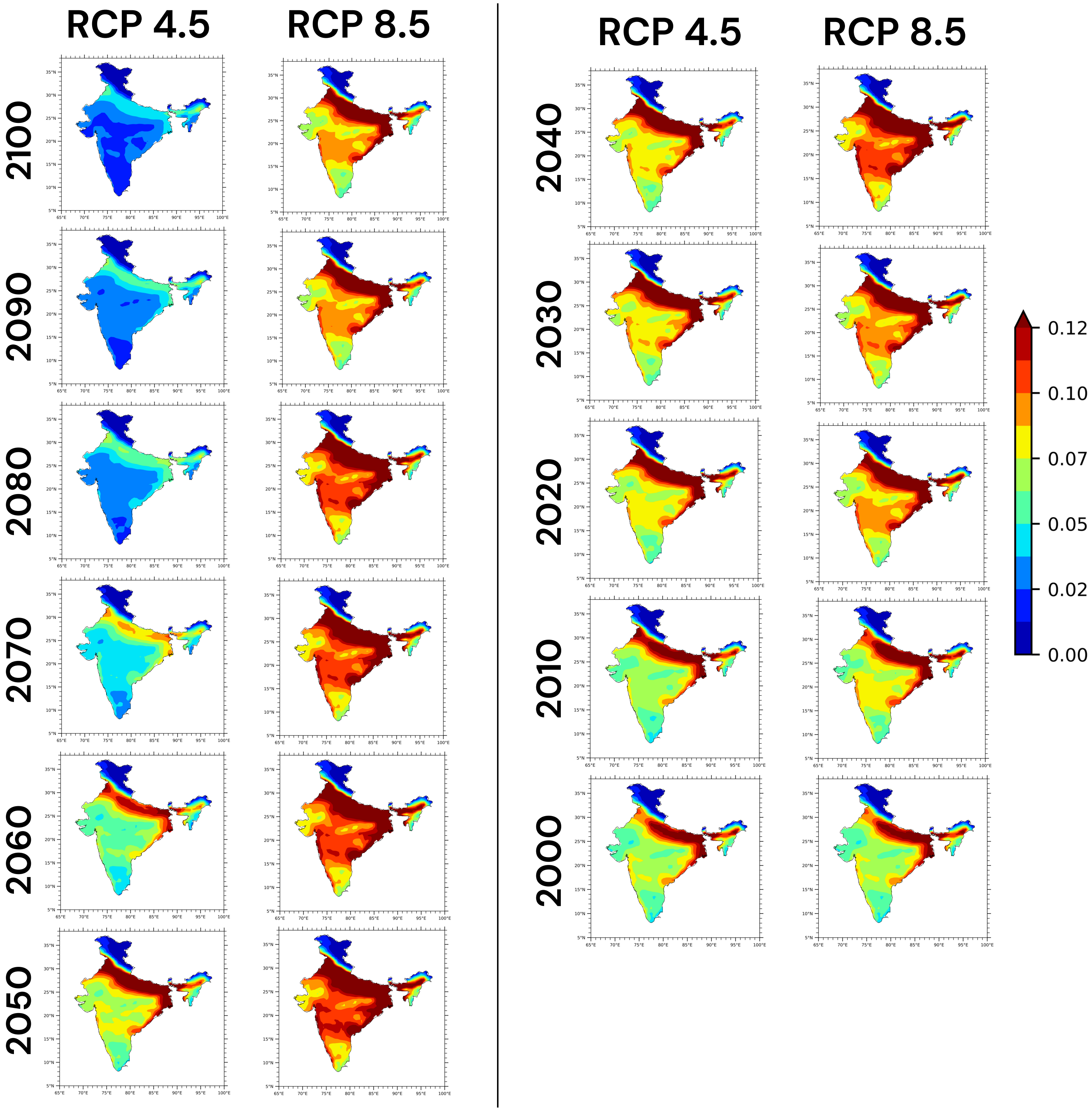

RCP 4.5
RCP 8.5
RCP 4.5
RCP 8.5
2100
2090
2080
2070
2060
2050
2040
2030
2020
2010
2000
0.12
0.10
0.07
0.05
0.02
0.00

Figure 9.

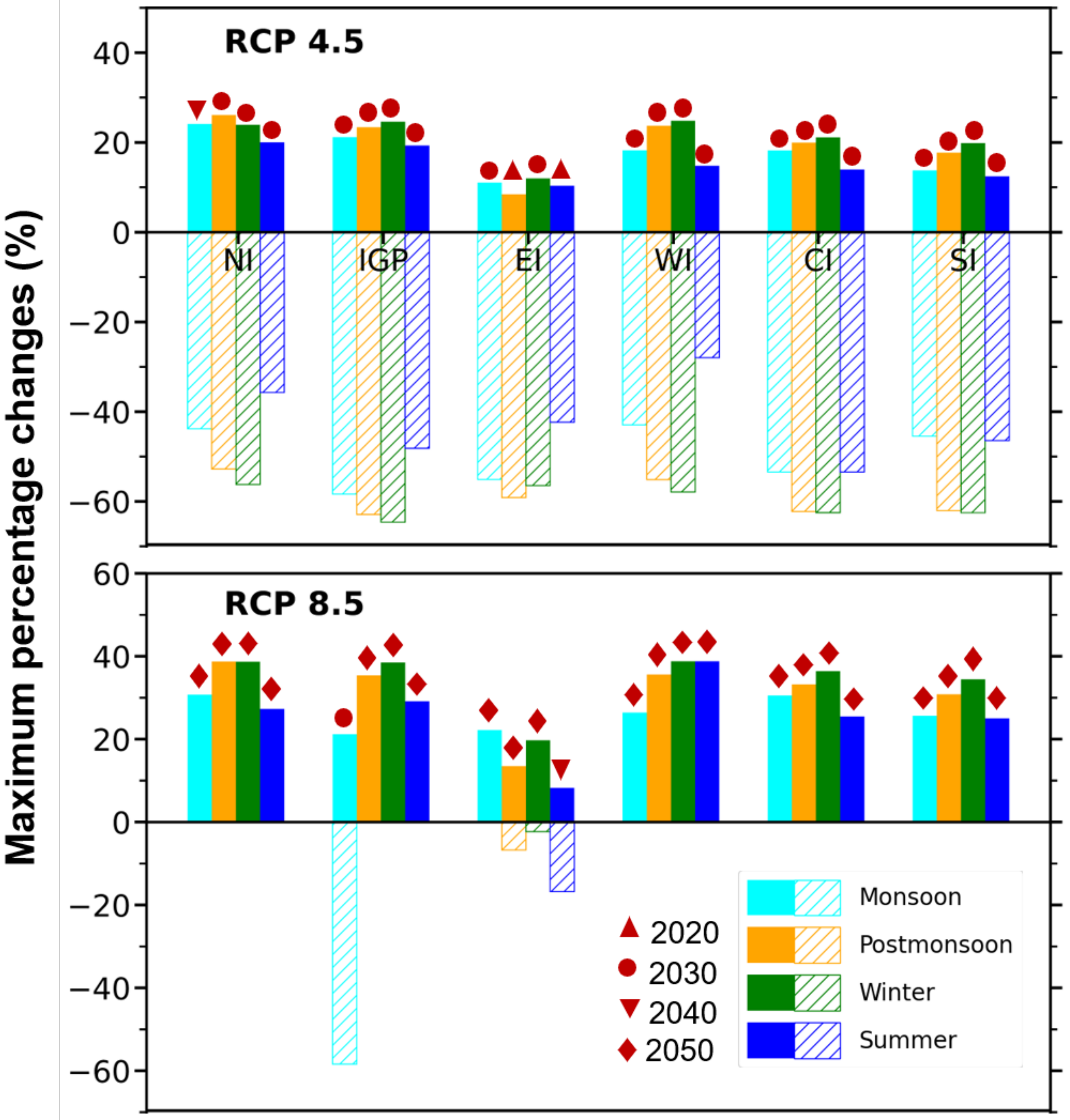

RCP 4.5
RCP 8.5
Maximum percentage changes (%)
40
20
0
−20
−40
−60
60
NI
IGP
EI
WI
CI
SI
2020
2030
2040
2050
Monsoon
Postmonsoon
Winter
Summer

Figure A1(a).

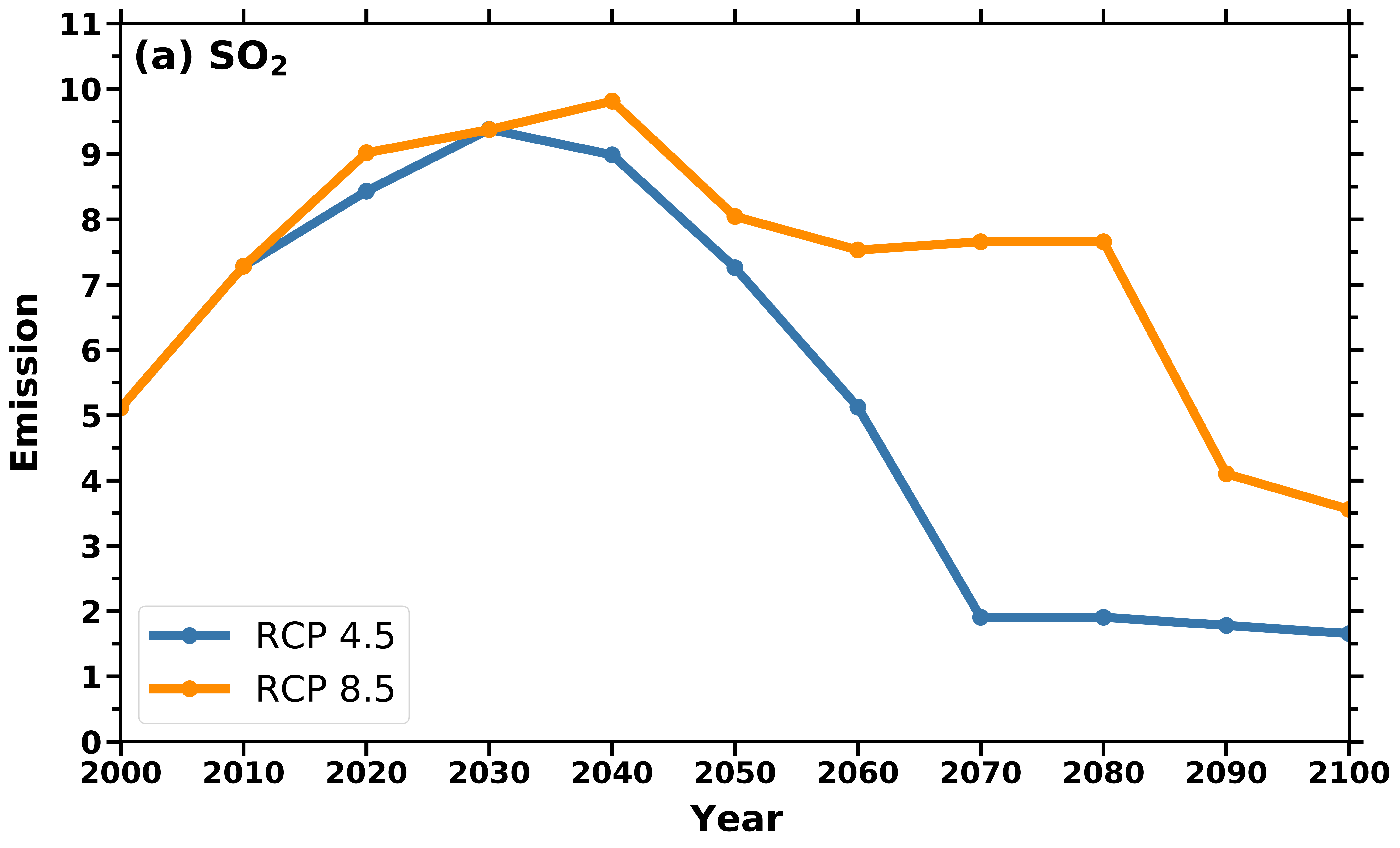

(a) SO_2
Emission
Year
RCP 4.5
RCP 8.5
0
1
2
3
4
5
6
7
8
9
10
11
2000
2010
2020
2030
2040
2050
2060
2070
2080
2090
2100

Figure A1(b).

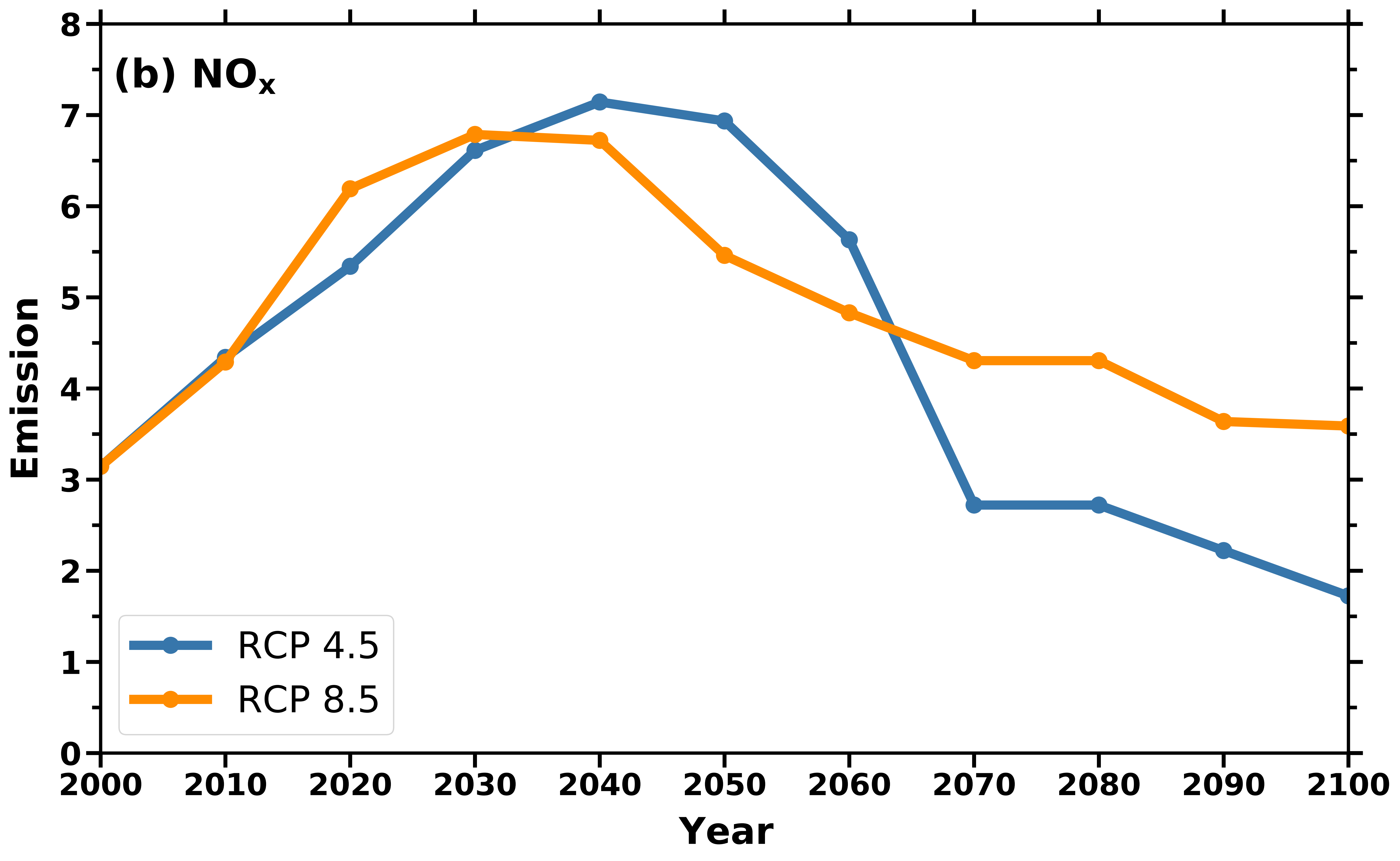

(b) NO_x
Emission
Year
RCP 4.5
RCP 8.5
0
1
2
3
4
5
6
7
8
2000
2010
2020
2030
2040
2050
2060
2070
2080
2090
2100

Figure A1(c).

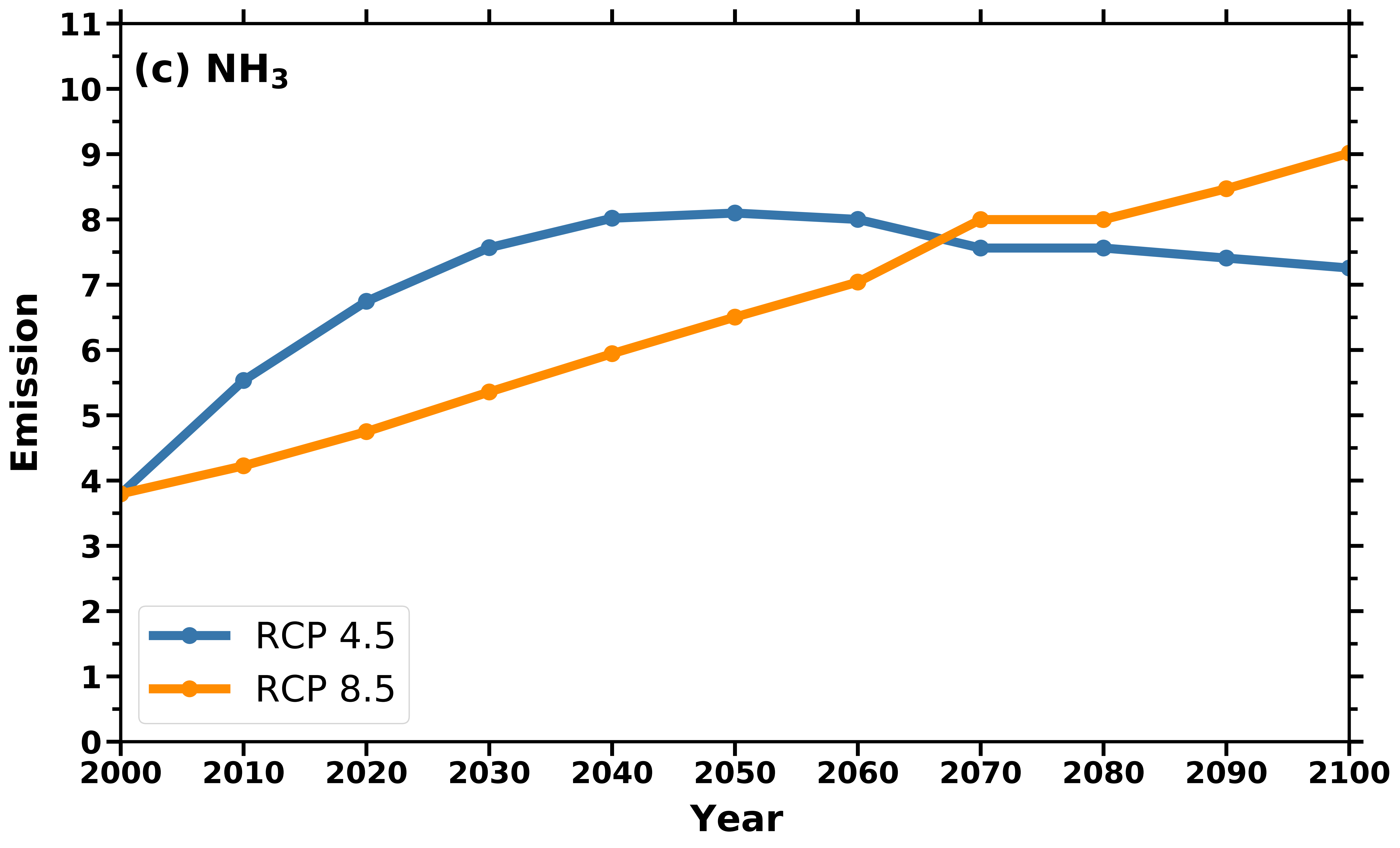

(c) NH_3
Emission
Year
0
1
2
3
4
5
6
7
8
9
10
11
2000
2010
2020
2030
2040
2050
2060
2070
2080
2090
2100
RCP 4.5
RCP 8.5

Figure A1(d).

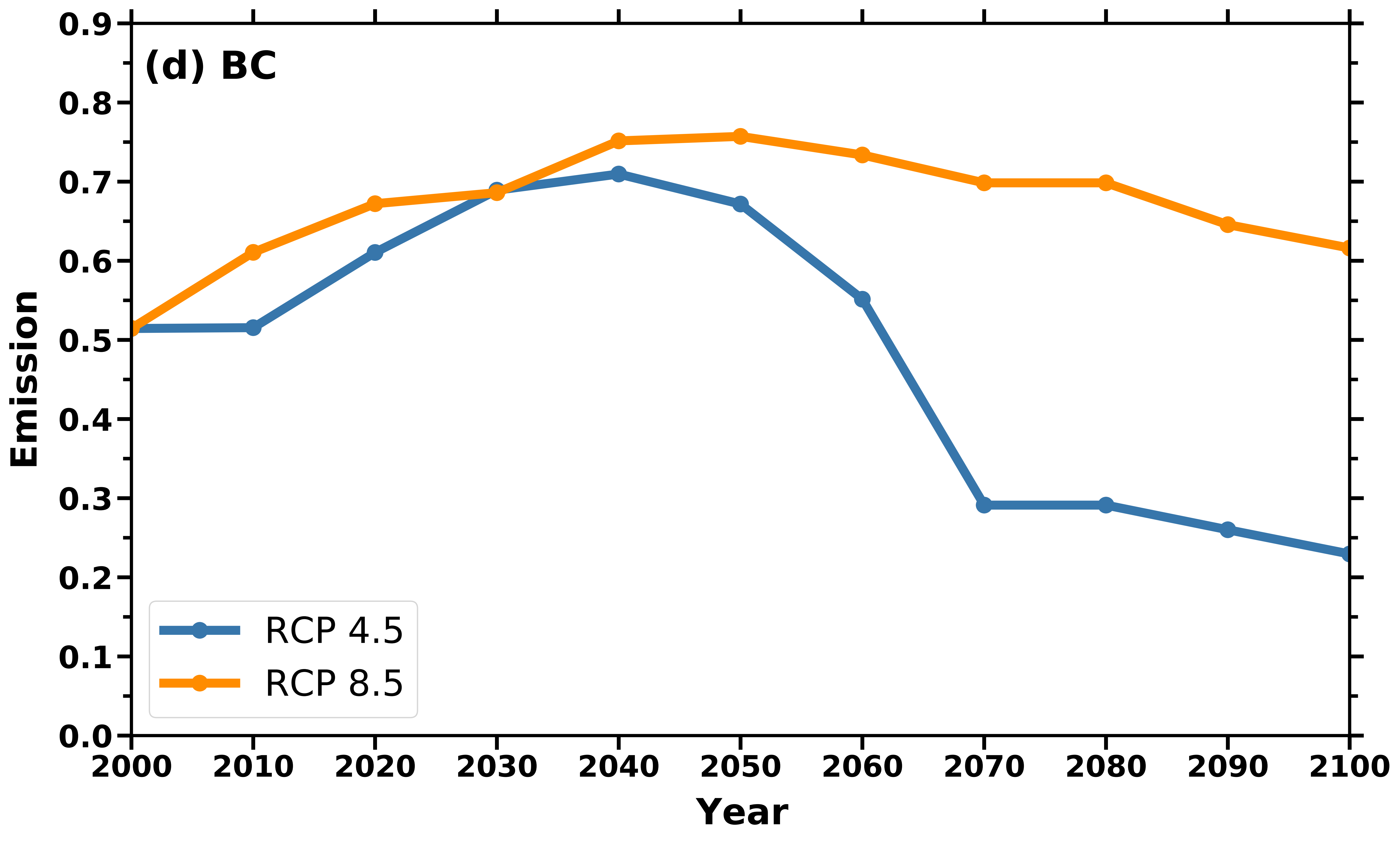
(d) BC
RCP 4.5
RCP 8.5
Emission
Year
0.0
0.1
0.2
0.3
0.4
0.5
0.6
0.7
0.8
0.9
2000
2010
2020
2030
2040
2050
2060
2070
2080
2090
2100

Figure A1(e).

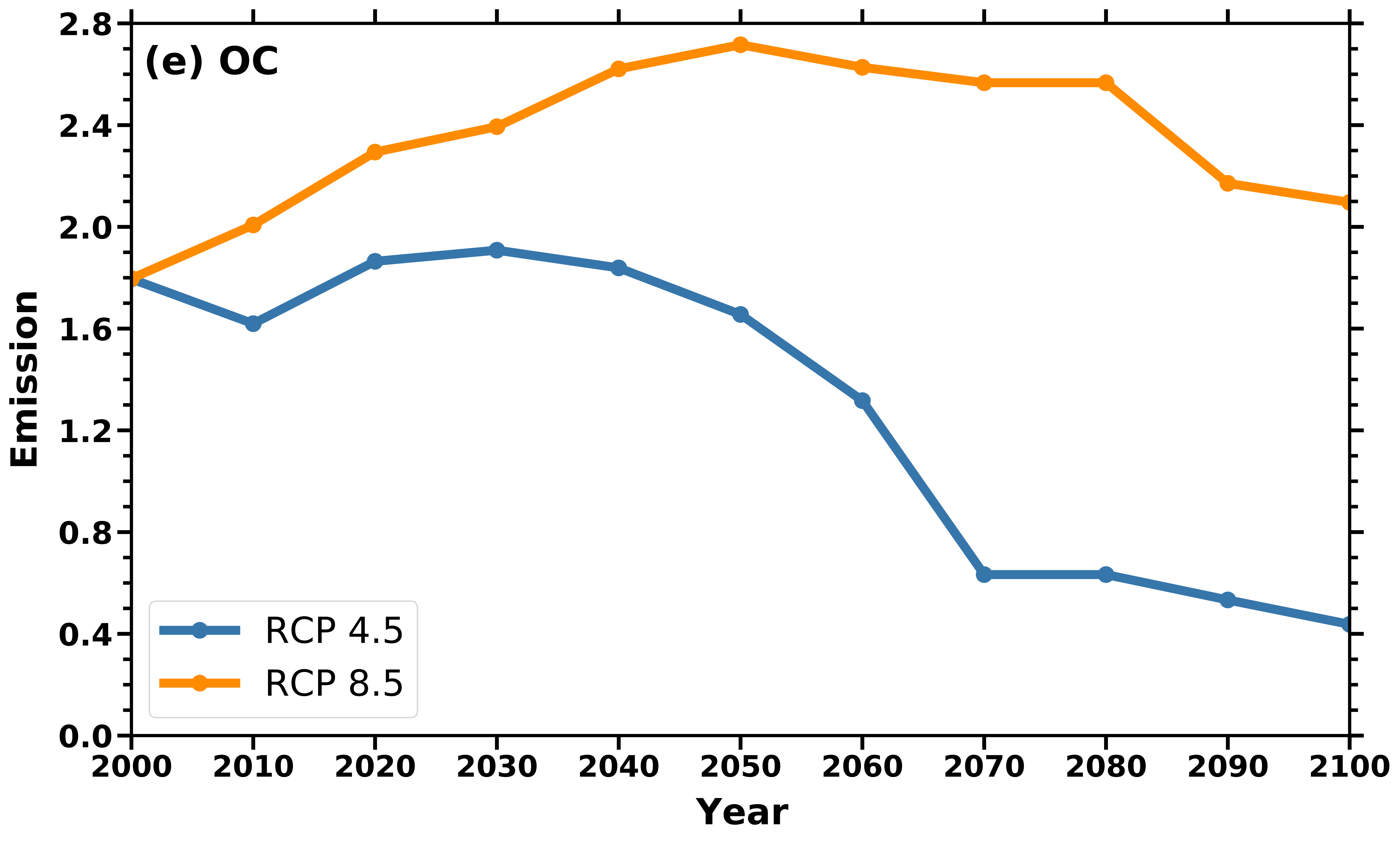
(e) OC
RCP 4.5
RCP 8.5
Emission
Year
0.0
0.4
0.8
1.2
1.6
2.0
2.4
2.8
2000
2010
2020
2030
2040
2050
2060
2070
2080
2090
2100

Figure A2.

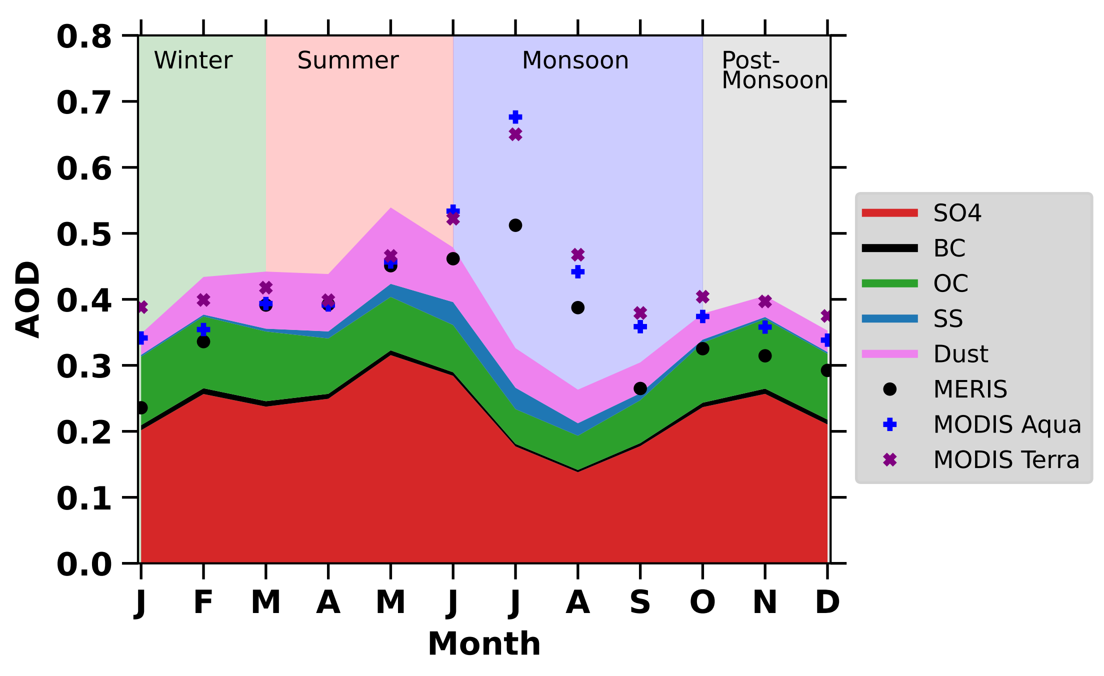

AOD
0.8
0.7
0.6
0.5
0.4
0.3
0.2
0.1
0.0
Winter
Summer
Monsoon
Post-
Monsoon
J
F
M
A
M
J
J
A
S
O
N
D
Month
SO4
BC
OC
SS
Dust
MERIS
MODIS Aqua
MODIS Terra

Figure A3.

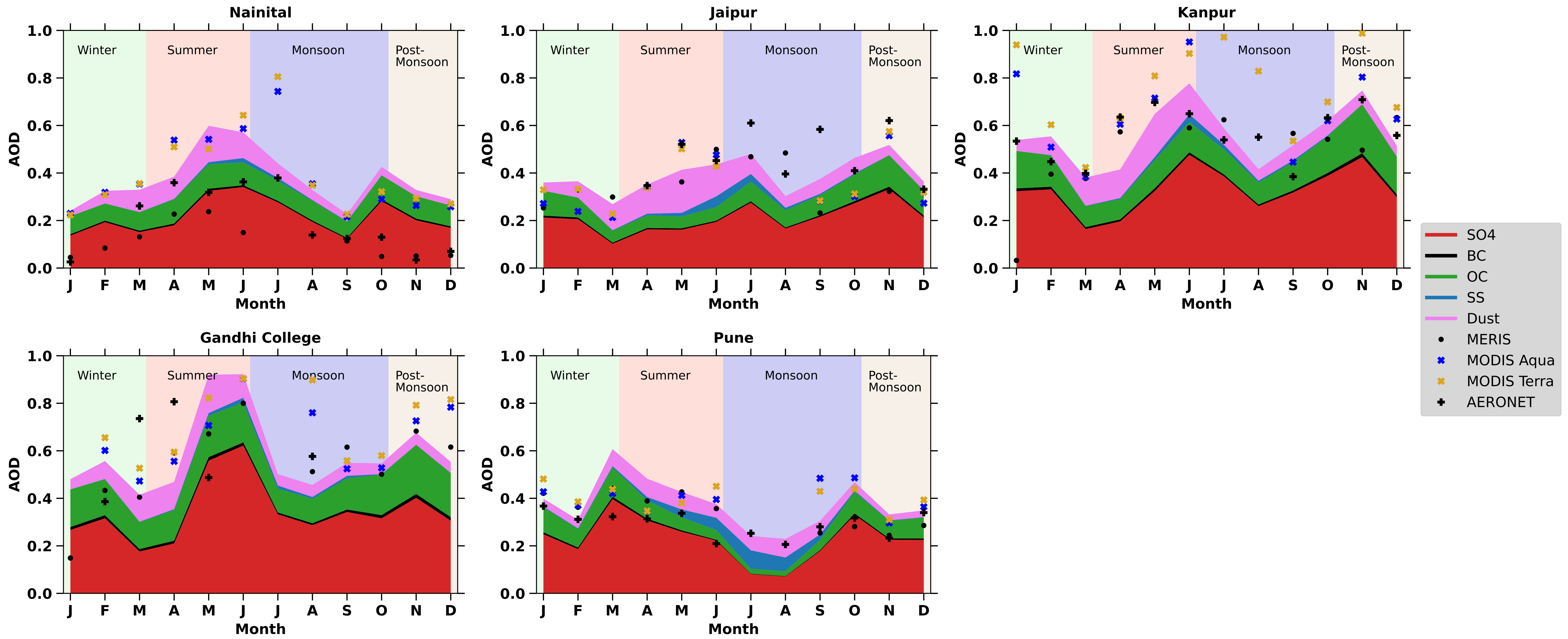

Nainital
Jaipur
Kanpur
Gandhi College
Pune
Winter
Summer
Monsoon
Post-Monsoon
AOD
Month
J F M A M J J A S O N D
SO4
BC
OC
SS
Dust
MERIS
MODIS Aqua
MODIS Terra
AERONET

Figure A4(a).

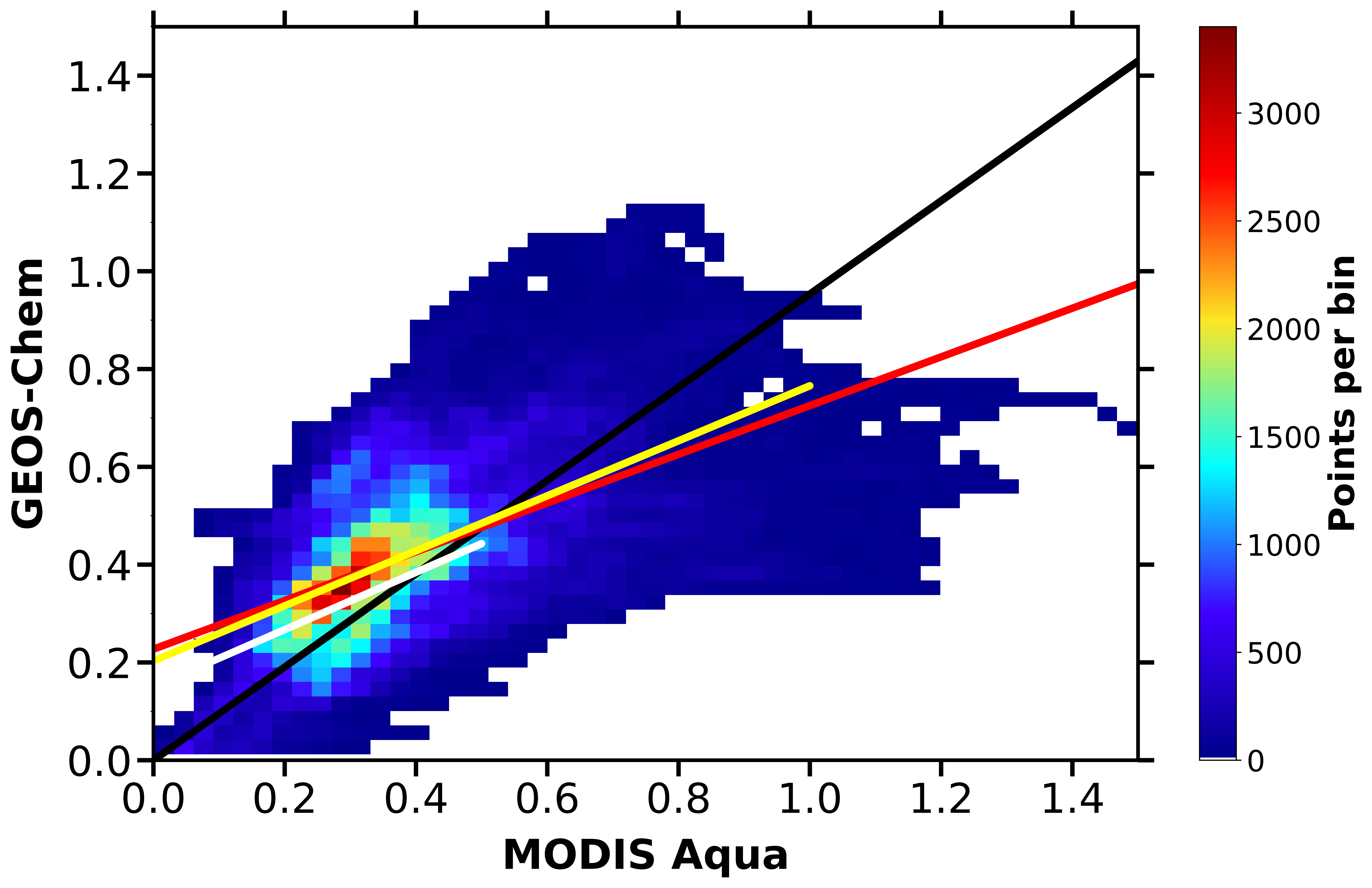

GEOS-Chem
MODIS Aqua
Points per bin
0.0
0.2
0.4
0.6
0.8
1.0
1.2
1.4
0
500
1000
1500
2000
2500
3000

Figure A4(b).

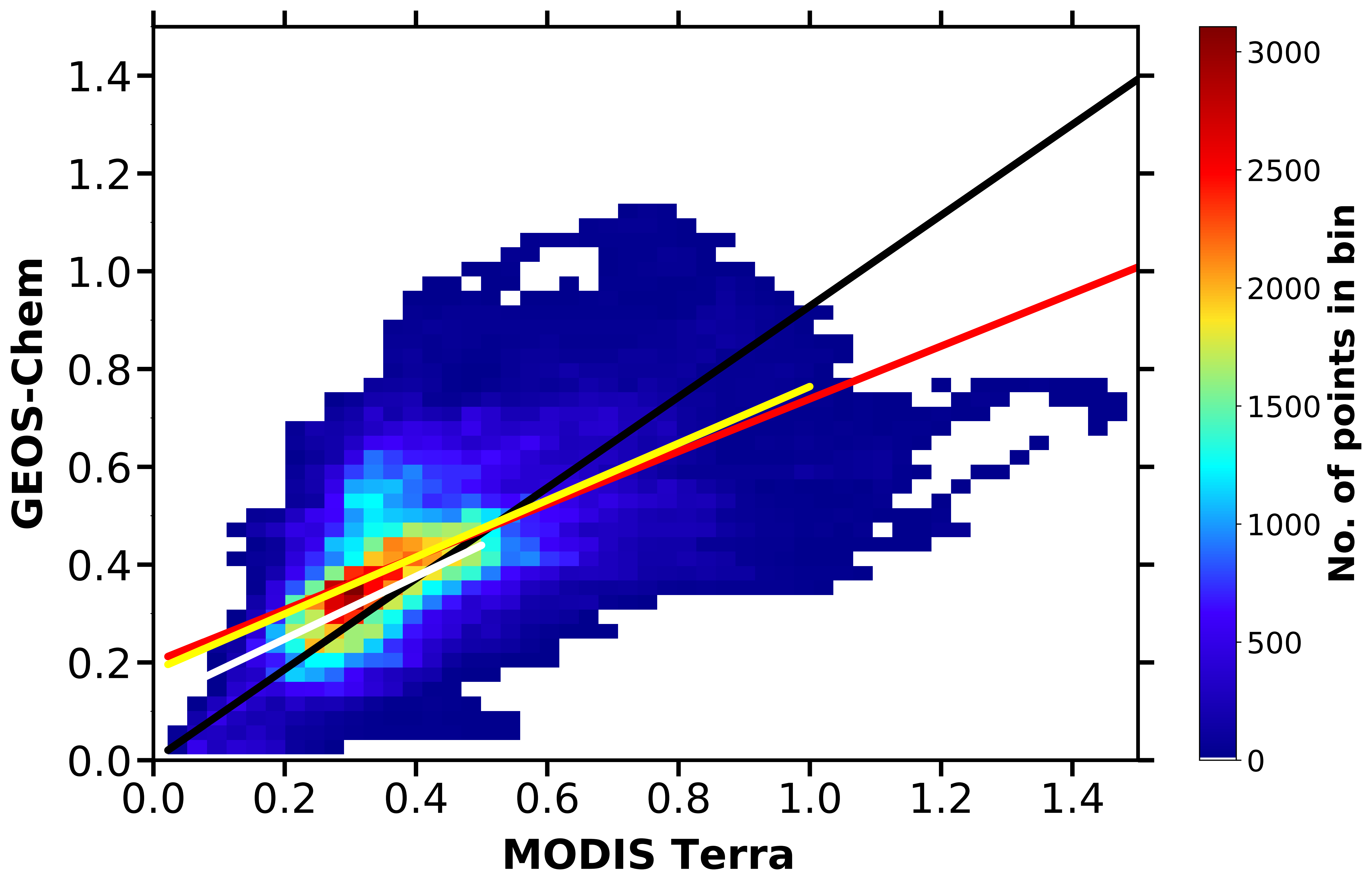

GEOS-Chem
MODIS Terra
No. of points in bin
0.0
0.2
0.4
0.6
0.8
1.0
1.2
1.4
0
500
1000
1500
2000
2500
3000

Figure A4(c).

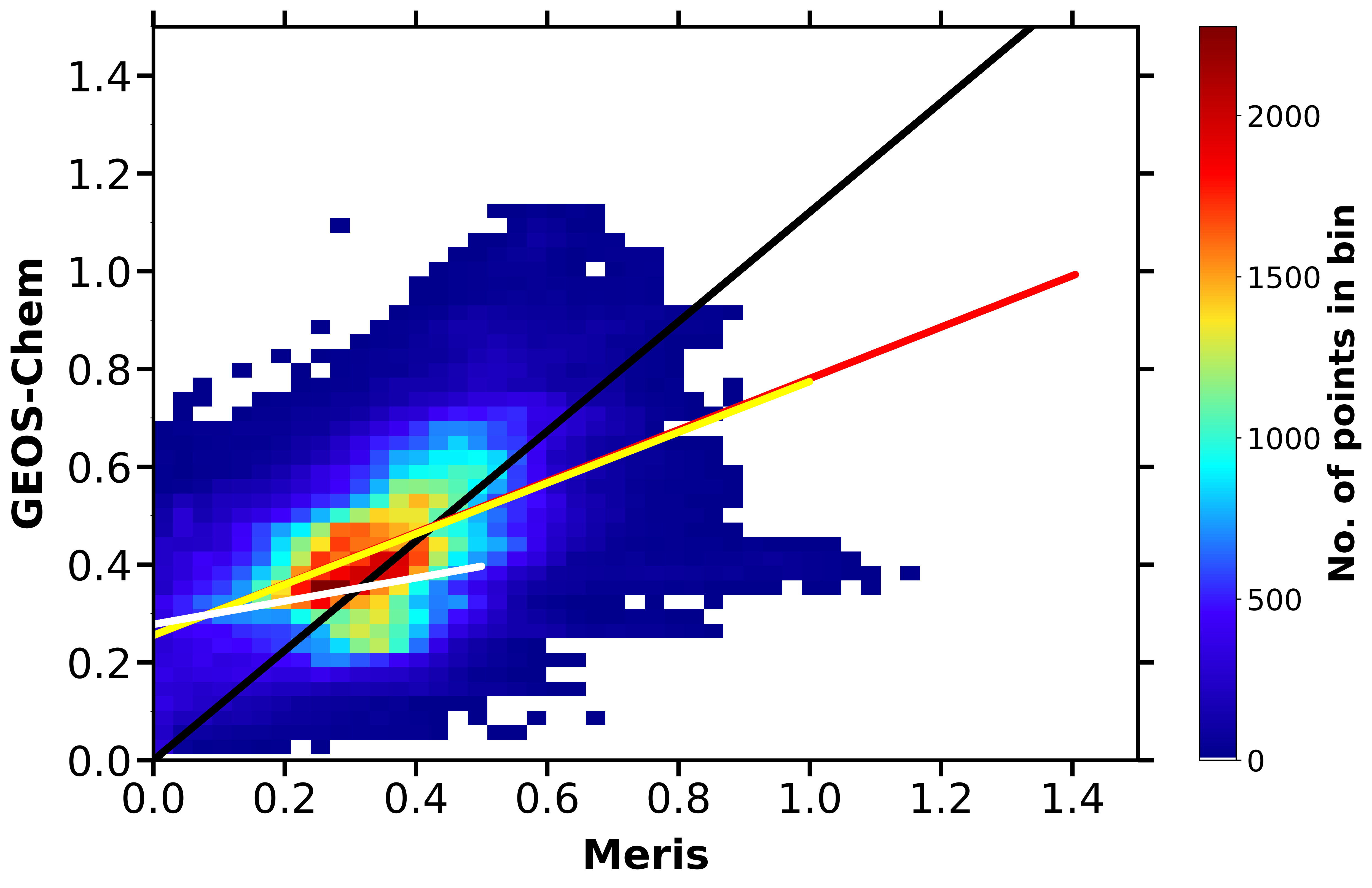
GEOS-Chem
Meris
No. of points in bin
0.0
0.2
0.4
0.6
0.8
1.0
1.2
1.4
0
500
1000
1500
2000

Figure A5.

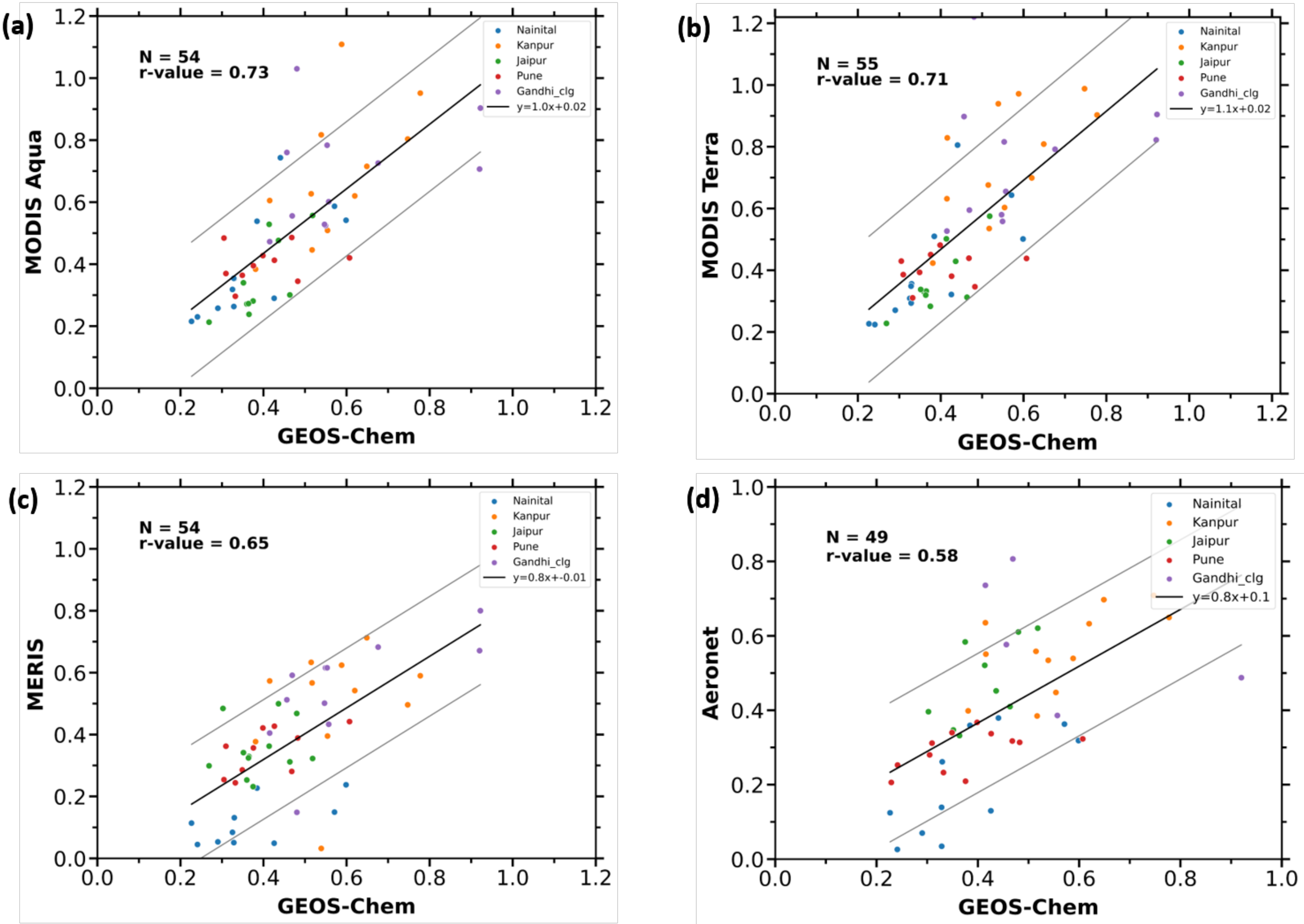
(a)
N = 54
r-value = 0.73
Nainital
Kanpur
Jaipur
Pune
Gandhi_clg
y=1.0x+0.02
MODIS Aqua
GEOS-Chem
(b)
N = 55
r-value = 0.71
Nainital
Kanpur
Jaipur
Pune
Gandhi_clg
y=1.1x+0.02
MODIS Terra
GEOS-Chem
(c)
N = 54
r-value = 0.65
Nainital
Kanpur
Jaipur
Pune
Gandhi_clg
y=0.8x+-0.01
MERIS
GEOS-Chem
(d)
N = 49
r-value = 0.58
Nainital
Kanpur
Jaipur
Pune
Gandhi_clg
y=0.8x+0.1
Aeronet
GEOS-Chem